

# **Electromagnetic wave absorbing properties of polymer composites**

Ing. Marek Gořalík, Ph.D.

Doctoral Thesis Summary



# Tomas Bata University in Zlín

## Faculty of Technology

Doctoral Thesis Summary

### **Vlastnosti polymerních kompozitů pohlcujících elektromagnetické vlny**

#### **Electromagnetic wave absorbing properties of polymer composites**

**Author:** Ing. Marek Gořalík, Ph.D.

Degree programme: Chemistry and Materials Technology (P2808)

Degree course: Technology of Macromolecular Compounds (2808V006)

Supervisor: Prof. Ing. Jarmila Vilčáková, Ph.D.

Consultant: Professor Extraordinary, MSc. Natalia Kazantseva, CSc.

External examiners: doc. Ing. et Ing. Ivo Kuřitka, Ph.D. et Ph.D.

doc. Dr. Ing. Vladimír Pavlínek

Prof. RNDr. Miroslav Raab, CSc.

Zlín, October 2022

© Marek Gořalík

Published by **Tomas Bata University in Zlín** in the Edition **Doctoral Thesis Summary**.

The publication was issued in the year 2022

Klíčová slova: *polymerní kompozitní materiály, elektrické a magnetické vlastnosti, reflexní ztráty, radioabsorbéry*

Keywords: *polymer composite materials, electrical and magnetic properties, reflection loss, radio-absorber*

Full text of the doctoral thesis is available in the Library of TBU in Zlín.

ISBN 978-80-7678-116-0

## ABSTRACT

This work is focused on the optimization of electromagnetic and mechanical properties of magnetic polymer composites for electromagnetic interference (EMI) applications as radio absorbers (RAs). Polymer composites with a dual-phase polymer matrix, vinyl-terminated polydimethylsiloxane (PDMS) in epoxy resin (ER), acrylonitrile-butadiene rubber (NBR), and a propylene-based thermoplastic elastomer (TPE) matrix were investigated for the fabricating of highly filled manganese-zinc ferrite (MnZn), carbonyl iron (CI), carbon black (CB) and carbon nanotube (CNT) composites with the goals of enhanced radio-absorption and mechanical properties. The dielectric and magnetic properties of the composites were determined by the type, concentration, and polymer matrix composition. Increasing the filler and PDMS concentration leads to an increase in magnetic losses due to a decrease in the demagnetizing field. The electromagnetic properties of the composites were investigated in the radio-frequency (RF) band using the impedance method (1 MHz – 3 GHz). Based on the complex permittivity ( $\epsilon^*$ ) and complex permeability ( $\mu^*$ ), the reflection loss RL (dB) of single-layer metal-backed RAs was calculated. The RAs with a MnZn ferrite and CI demonstrated better bandwidth performance in comparison with RAs based on carbon fillers due to a proper ratio between  $\epsilon^*$  and  $\mu^*$ . According to the dynamical-mechanical analysis (DMA) and Charpy impact strength, the significant increase of stiffness up to 125% and the impact strength up to 150% was achieved due to the optimal composition of the polymer matrix and the filler. The results obtained in the study indicate the possibilities of the preparation of ER and elastomeric magnetic composites able to shield electromagnetic field by the absorption mechanisms.

## ABSTRAKT

Tato práce je zaměřena na optimalizaci elektromagnetických a mechanických vlastností magnetických polymerních kompozitů jako radioabsorbérů pro aplikace v oblasti elektromagnetické interference (EMI). Polymerní kompozity s dvoufázovou polymerní maticí, obsahující polydimethylsiloxan (PDMS) v epoxidové pryskyřici (ER) byly využity pro výrobu vysoce plněných kompozitů s mangano-zinečnatým feritem (MnZn) a karbonylovým železem (CI) s ohledem na radioabsorpční a mechanické vlastnosti. Dále byly připraveny elastomerní kompozity s maticí akrylonitril-butadienového kaučuku (NBR) a termoplastického elastomeru na bázi propylenu (TPE) s plnivem sazí (CB), uhlíkových nanotrubiček (CNT), MnZn a CI. Dielektrické a magnetické vlastnosti kompozitů byly určeny typem, koncentrací a složením polymerní matrice. Zvýšení plniva a koncentrace PDMS vedlo ke zvýšení magnetických ztrát v důsledku poklesu demagnetizačního pole. Elektromagnetické vlastnosti kompozitů byly sledovány v radio-frekvenčním (RF) pásmu s pomocí impedanční metody (1 MHz – 3 GHz). Na základě komplexní permitivity ( $\epsilon^*$ ) a komplexní permeability ( $\mu^*$ ) byla vypočtena ztráta odrazem RL (dB) jednovrstvých radioabsorbérů. Kompozity plněné MnZn a CI prokázaly větší poměr šířky operačního pásma k tloušťce ve srovnání s radioabsorbérem na bázi CB a CNT, a to díky správnému poměru mezi komplexní permitivitou ( $\epsilon^*$ ) a permeabilitou ( $\mu^*$ ). Při optimálním složení polymerní matrice (ER/PDMS) a plniva bylo dosaženo výrazného zvýšení tuhosti (125%) a rázové houževnatosti (150%) na základě dynamicko-mechanické analýzy (DMA) a rázové zkoušky ve srovnání čistou pryskyřicí. Výsledky, které byly získané při řešení práce poukazují na možnost přípravy magnetických kompozitů na bázi ER a elastomerní matrice, schopných stínit elektromagnetické záření absorpčními mechanismy.

# CONTENTS

<b>1. THEORETICAL BACKGROUND</b>	<b>7</b>
<b>1.1 INTRODUCTION TO EMI SHIELDING COMPOSITES</b>	<b>7</b>
<b>1.2 POLYMER MATRIX</b>	<b>8</b>
<b>1.3 FILLERS</b>	<b>10</b>
1.3.1 MAGNETIC FILLERS	10
1.3.2 CARBON-BASED FILLERS	10
<b>1.4 ELECTROMAGNETIC WAVE ABSORBERS</b>	<b>11</b>
1.4.1 APPLICATION OF ELECTROMAGNETIC WAVE ABSORBERS	12
<b>1.5 EMI SHIELDING MECHANISM</b>	<b>12</b>
1.5.1 CALCULATION OF REFLECTION LOSS	13
1.5.2 CALCULATION OF SHIELDING EFFECTIVENESS	14
<b>1.6 MEASUREMENT TECHNIQUES</b>	<b>15</b>
1.6.1 DIELECTRIC AND MAGNETIC PROPERTIES	15
1.6.2 S-PARAMETERS MEASUREMENT	15
<b>2. AIMS OF THE THESIS</b>	<b>17</b>
<b>3. EXPERIMENTAL SECTION</b>	<b>18</b>
<b>3.1 MATERIALS</b>	<b>18</b>
<b>3.2 SAMPLE PREPARATION</b>	<b>19</b>
3.2.1 POLYMER BLEND PREPARATION	19
3.2.2 FABRICATION OF THE ER/PDMS/MnZn AND ER/PDMS/CI BLENDS	19
3.2.3 PREPARATION OF THE NBR/MnZn, NBR/CB AND NBR/CNT ELASTOMER COMPOSITES	20
3.2.4 PREPARATION OF THE TPE/MnZn AND TPE/CI COMPOSITES	20
<b>3.3 CHARACTERIZATION TECHNIQUES</b>	<b>20</b>
<b>4. RESULTS AND DISCUSSION</b>	<b>22</b>
<b>4.1 MORPHOLOGY</b>	<b>22</b>
4.1.1 THE ER/PDMS/MnZn AND CI COMPOSITES	22
4.1.2 THE NBR/MnZn COMPOSITES	22

4.1.3 THE NBR/CB/MnZn COMPOSITES	22
4.1.4 THE NBR/CB AND NBR/CNT COMPOSITES	23
4.1.5 THE TPE/MnZn AND TPE/CI COMPOSITES	23
<b>4.2 DIELECTRIC AND MAGNETIC PROPERTIES</b>	<b>24</b>
4.2.1 THE COMPLEX PERMITTIVITY OF ER/PDMS COMPOSITES	24
4.2.2 THE COMPLEX PERMITTIVITY OF NBR/MnZn AND HYBRID NBR/CB/MnZn COMPOSITES	25
4.2.3 THE COMPLEX PERMEABILITY OF ER/PDMS COMPOSITES	25
4.2.4 THE COMPLEX PERMEABILITY OF NBR/MnZn AND NBR/CB/MnZn COMPOSITES	27
<b>4.3 ELECTROMAGNETIC SHIELDING CHARACTERISTICS OF COMPOSITES</b>	<b>28</b>
4.3.1 RL OF THE ER/PDMS/MnZn AND ER/PDMS/CI COMPOSITES	28
4.3.2 RL OF THE NBR/MnZn AND NBR/CB/MnZn HYBRID COMPOSITES	29
4.3.3 RL OF THE TPE/MnZn AND TPE/CI COMPOSITES	30
<b>4.4 MECHANICAL PROPERTIES</b>	<b>30</b>
4.4.1 DMA OF THE ER/PDMS/MnZn, ER/PDMS/CI AND NBR/CB COMPOSITES	30
4.4.2 TENSILE PROPERTIES OF THE NBR AND TPE COMPOSITES	32
4.4.3 DC CONDUCTIVITY OF THE ER/PDMS, NBR AND TPE COMPOSITES	32
<b>5. SUMMARY OF THE RESULTS</b>	<b>34</b>
<b>6. CONCLUSION</b>	<b>36</b>
<b>REFERENCES</b>	<b>37</b>
<b>LIST OF FIGURES</b>	<b>43</b>
<b>LIST OF TABLES</b>	<b>44</b>
<b>LIST OF SYMBOLS AND ABBREVIATIONS</b>	<b>45</b>
<b>CURRICULUM VITAE</b>	<b>47</b>
<b>LIST OF PUBLICATIONS</b>	<b>48</b>

# 1. THEORETICAL BACKGROUND

## 1.1 Introduction to EMI shielding composites

The high-frequency electromagnetic wave has increasingly attracted attention due to the rapid development of telecommunication devices for supporting 4G/5G wireless systems and aircraft applications. Various communication devices such as smartphones, router and electronic components are capable of producing a high-frequency electromagnetic wave, which emits into the surroundings. The electromagnetic wave may interrupt electronic devices, leak information, and threaten public health [1, 2].

In the high-frequency and microwave regions, thermal effects occur that lead to heating of living tissue. A substance with a high heating factor results in a small penetration depth of microwaves, because the energy is converted into heat already in its outer layers. Hirata, 2010 [2] argues that a whole-body averaged SAR below 0.08 W/kg is not hazardous to human health.

Previously, metal plates were used as screens due to their high electrical conductivity [3]. The high performance of electromagnetic polymer composites (EPC) is the result of low weight and density along with high strength and toughness. EPCs can be used to obtain radio-absorbing material (RAM), reducing the reflection of incident electromagnetic waves due to dielectric and/or magnetic losses. From the point of view of electrodynamics, a more efficient absorption of electromagnetic radiation can be achieved by using RAMs with high permeability, high magnetic loss, a favourable form of frequency dependence of complex permeability ( $\mu^*$ ) and complex permittivity ( $\epsilon^*$ ), and a proper ratio between the permeability and the permittivity in a certain frequency range [6]. Common RAMs used for RAs are plastics and elastomers, as well as composites containing conductive and magnetic fillers [4, 5, 6, 7].

The aim of this thesis is the optimization of electromagnetic and mechanical properties of magnetic polymer composites and elastomeric composites (NBR, TPE), and composites for EMI applications in the radio-frequency band. To this end, highly filled magnetic polymer composites with a dual-phase polymer matrix, vinyl-terminated polydimethylsiloxane (PDMS) in epoxy resin (ER), an elastomeric (NBR) and thermoplastic (TPE) matrix were fabricated. As filler, MnZn, CI, CB and CNT fillers were used. The electromagnetic properties of the composites were evaluated in the RF band using the impedance method. Based on the complex permittivity ( $\epsilon^*$ ) and the complex permeability ( $\mu^*$ ), the RL (dB) of single-layer RAs were calculated.



## 1.2 Polymer matrix

The primary purpose of the polymer matrix in composites is to bind the filler particles together, owing to its cohesive and adhesive characteristics, while the filler particles are responsible for the electromagnetic properties of the composite [8]. Generally, polymer matrixes are classified as thermoplastic, thermosetting polymers and elastomers.

*Thermoplastics* consist of linear or branched chain molecules having strong intramolecular bonds but weak intermolecular bonds. Fig. 1 shows the dependence of Young's modulus ( $E$ ) on the density ( $\rho$ ) of materials (polymers, elastomers and composites). Polymers have the value of  $E$  in the range from 1 GPa to 20 GPa. Polymer composite materials have a higher stiffness and receive the value of  $E$  (12 – 200 GPa); the values of density are in the range (1300 – 1800 kg/m<sup>3</sup>).

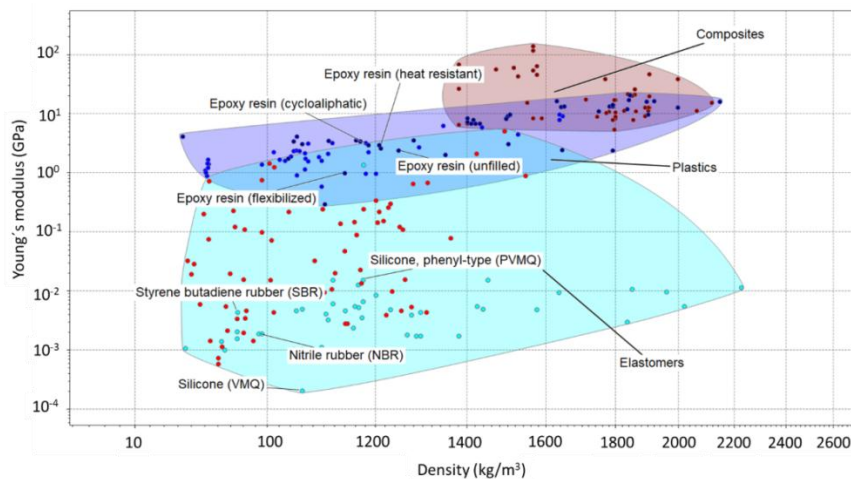


Figure 1: Dependence of Young's modulus on density

*Thermosets* have cross-linked or network structures with covalent bonds among all molecules. They do not soften but decompose on heating. Common examples are epoxies, polyesters, phenolic, ureas, melamine resins, and silicone.

*Epoxy resins (ER)* are a group of viscous liquids containing a molecule epoxide group (oxirane) consisting of an oxygen atom attached to two connected carbon atoms. With regard to the low weight requirement of the composite, the epoxy resin reached the value of density in the interval from 1150 to 1250 kg/m<sup>3</sup> with value  $E$  (3 – 6 GPa). It therefore seems to be a suitable matrix for the preparation of magnetic polymer composites (Fig. 1).

Fig. 2 shows the dependence of tensile strength on price (CZK/kg) of materials. The price of epoxy resin is in the range of (50 – 80 CZK/kg), while maintaining a sufficiently high tensile strength with value (60 – 100 MPa). This matrix shows a good price-tensile strength ratio.

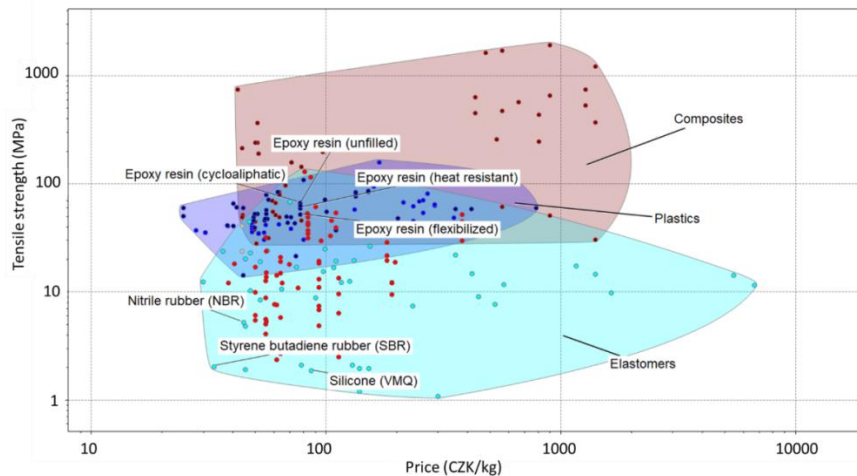


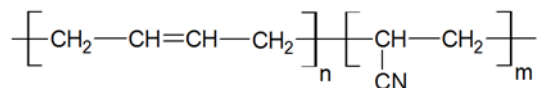
Figure 2: Dependence of tensile strength on price (CZK/kg)

### Elastomers

Elastomers are polymers that are held together by weak intermolecular forces, generally exhibiting low Young's modulus (0.01 – 1 GPa) and tensile strength (1 – 100 MPa). Examples of elastomers include natural rubber, polyurethanes, polybutadiene, silicone, and neoprene.

#### Acrylonitrile-butadiene rubber (NBR)

*Chemical formula:*



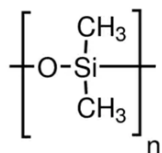
*Operating temperature range:* -50 – 150°C; *Typical hardness:* Shore “A” 66;

*Advantages:* Excellent resistance to oil and benzene; superior resistance to petroleum-based hydraulic fluids; good high-temperature performance.

*Limitations:* Poor resistance to oxygenated solvents.

#### Poly(dimethylsiloxane)

*Chemical formula:*



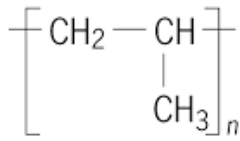
*Operating temperature range:* -60 – 370°C; *Typical hardness:* Shore “A” 60 – 70.

*Advantages:* Outstanding heat resistance; excellent flexibility at low temperature; excellent resistance to weather, ozone, sunlight, and oxidation.

*Limitations:* Fair resistance to oil benzene and solvents.

Isostatic propylene (iPP)

*Chemical formula:*



*Operating temperature range:* -30 – 130°C; *Typical hardness:* Shore “A” 67.

*Advantages:* Suitable for a wide range of blown and cast film applications, extrusion coating and lamination applications.

*Limitations:* degradation from exposure to heat and UV radiation.

## 1.3 Fillers

### 1.3.1 Magnetic fillers

Materials with electrical and/or magnetic dipoles suitable for shielding applications in which absorption is the dominant shielding mechanism [9–12]. The most widespread magnetic fillers in magneto-polymeric composites are soft and hard ferrites (MnZn, NiZn, Co<sub>2</sub>Z, Co<sub>2</sub>W, etc.) and CI powders. Electrically conductive filler, such as metal powder, CB [13, 14] and CNT are used to achieve high electrical conductivity of the composite [15].

*Manganese-zinc ferrite (MnZn)*

Ferrite consists of 53.75 mol % of Fe<sub>2</sub>O<sub>3</sub>, 26.10 mol % of MnO, and 20.15 mol % of ZnO. This ferrite is characterized by the initial permeability  $\mu_i \sim 3000$ -5000, the Curie temperature  $T_C = 473$  K [45], the conductivity  $\sigma_f = 2 \times 10^{-2}$  S/m, the density  $\rho_f = 4.8$  g/cm<sup>3</sup>, specific surface area (10.99 m<sup>2</sup>/g) and cost-efficiency. It has high values of resistivity, permeability, and permittivity.

*Carbonyl Iron (CI)*

Soft magnetic, CI powders are widely used as a filler of radio and microwave absorbers due to saturation magnetization 1659 kA/m and broad bandwidth 2–18 GHz [16]. In particular, the relatively high density of CI (7.9 g/cm<sup>3</sup>) makes it possible to achieve high filler content, and thus improve the electromagnetic absorbing properties of the composites. The disadvantage of CI is its rapid oxidation in the air which affects its magnetic properties. To prevent oxidation, CI particles are modified by coating with SiO<sub>2</sub> or conducting polymers [17, 18].

### 1.3.2 Carbon-based fillers

Carbon-based fillers exhibit unique properties such as high permittivity, excellent electrical conductivity, low density, high mechanical, chemical and thermal stability, as well as excellent physical properties. In addition, due to their diverse structure they also improve their physic-mechanical and dynamic

properties.

### *Carbon nanotubes (CNT)*

Carbon nanotubes (CNTs) are an allotropic modification of carbon. They consist of one (SWCNT) or more (MWCNT) graphite layers. The structure of CNT is achieved by rolling the graphite layer into a cylindrical or tubular shape. This efficient behaviour is caused by excellent electrical properties and very high aspect ratios  $p$  ( $p=L/d$ , where  $L$ = length, 1 – 50  $\mu\text{m}$  and  $d$ -diameter, 1-50 nm). They have electrical conductivity of  $10^0 - 10^1$  S/cm, low apparent density, high surface area, porosity, gas permeability and excellent mechanical properties: high tensile strength (13 – 53 GPa) and Young's modulus (1000 – 5000 GPa) [19, 20].

### *Carbon black*

Carbon black (CB) is the most widely used carbon-based filler in the rubber industry, mainly due to its low cost, easy production and suitable physical properties [21]. CB is a form of paracrystalline carbon that has a high surface area to volume ratio. It may be partially graphitic with onionskin structure, each layer being graphitic (hexagonal organization of carbon atoms). Domain structures of CB are: particle ( $\sim 50$  nm), aggregate ( $\sim 1$   $\mu\text{m}$ ) and agglomerate ( $\sim 10$   $\mu\text{m}$ ). Electrical conductivity of dry compressed CB is of the order  $10^4$  S/cm with density in the range (1.7 – 1.9  $\text{g/cm}^3$ ).

## **1.4 Electromagnetic wave absorbers**

Electromagnetic wave absorbers are devices that convert the energy of incident electromagnetic radiation to heat via conductive, dielectric, and/or magnetic losses. In general, the performance of EM wave absorbing materials depends on EM attenuation capability and impedance matching characteristics [22, 23]. Several types of EWAs absorbers are used, as shown in Fig. 3.

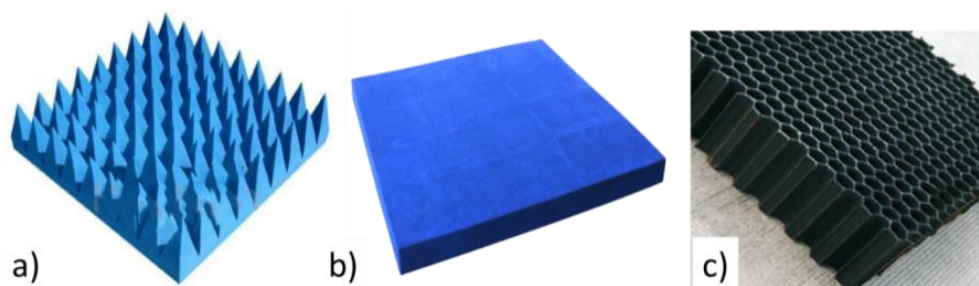


*Figure 3: EWAs: a) pyramidal type, b) plane type, c) honeycomb type*  
[52, 53]

### *Classifications of EWAs*

Electromagnetic wave absorbers can be divided into dielectric absorbers and magnetic absorbers. Dielectric absorbers (CB and CNT) are materials with a low

permeability  $\mu'$ , and they are matched with free space by using the resonance thickness. The typical dielectric absorbers are composite materials consisting of a conductive filler. Ferrites as MnZn and CI are the most frequently used in RAM, because it due to the combination of electric loss and magnetic loss [24].

### 1.4.1 Application of electromagnetic wave absorbers

EM waves can be classified into extremely low frequency (ELF), radio frequency, and microwave radiation depending on the wavelength range (Fig. 4). Generally, EM wave frequencies in the range of 3 to 3000 Hz are generated from the electric wires and electronics used in workplaces and homes [25].

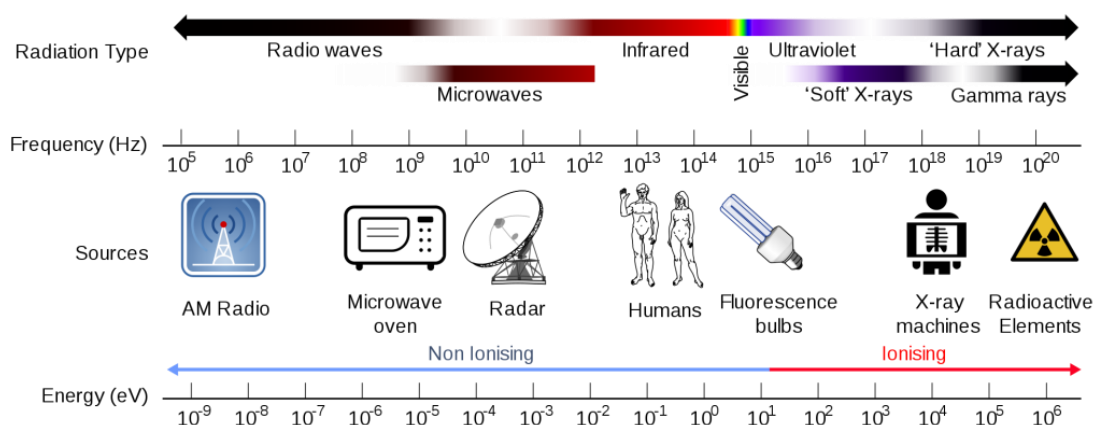


Figure 4: EM band applications in the (RF) and (MW) range [54].

An electromagnetic field is emitted from devices such as radio, Wi-Fi systems, mobile phones, satellite communication systems, and TV stations. The most promising use of the absorbers are in the field of defence and aeronautics, where they are employed in stealth technology [26, 27], avionics cover surfaces [28, 29]. Other areas of applications of EWAs are in the field of consumer and industrial electronics [30, 31, 32].

## 1.5 EMI shielding mechanism

Shielding of electromagnetic radiation is achieved using three mechanisms: reflection, absorption and multi-reflection.

The reflection of radiation for EMI shielding is the primary function by using charge carriers, which directly related to interaction of electromagnetic waves with a shielding material. Absorption of EM radiation is the second element for EMI shielding, the principle of which is that the material's electric and magnetic dipoles interact with the radiation [33]. Multiple reflections are another probable interaction of the electromagnetic waves with the material, which takes place when waves reflect from encountered surfaces. The interaction of electromagnetic waves with the material is illustrated in Fig. 5.

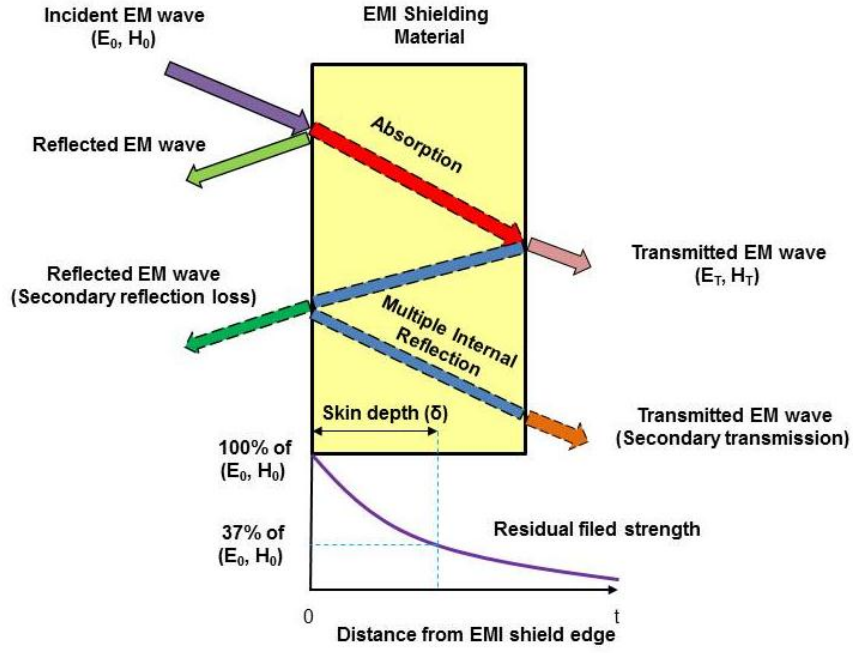


Figure 5: The interaction of electromagnetic waves with the material.

### 1.5.1 Calculation of reflection loss

For a single-layer RA (Fig. 5), the absorption of electromagnetic energy is a function of frequency. The reflection loss (RL) can be evaluated from the measured magnetic and dielectric spectra and the RA thickness by the following equations:

$$RL = 20 \log \left| \frac{Z - Z_0}{Z + Z_0} \right| \quad (1)$$

in which the normalized input impedance can be computed according to the transmission-line theory. To satisfy the minimum reflection loss, according to Eq.1 the perfect matching condition is,

$$Z = j \sqrt{\frac{\mu}{\epsilon}} \tan \left( \frac{2\pi f}{c} \sqrt{\mu^* \epsilon^*} d \right) \quad (2)$$

where  $Z$  is the input impedance of the layer,  $Z_0$  is the wave impedance of the free space;  $f$  is the frequency;  $c$  is the velocity of the light;  $d$  is the layer thickness;  $\epsilon^*$  and  $\mu^*$  are complex relative permittivity and permeability.

If the condition  $Z=1$  is fulfilled, the reflection from the RA is absent. To find these conditions in RAMs, a numerical procedure close to a graphical procedure is usually applied to find the matching frequency  $f_0$  and the matching thickness  $d_0$  [34]. The complex permittivity ( $\epsilon'$  and  $\epsilon''$ ) and the complex permeability ( $\mu'$  and  $\mu''$ ) are important EM parameters for evaluating the microwave absorption

performance. The  $\varepsilon'$  and  $\varepsilon''$  are related to the dielectric properties, and the  $\mu'$  and  $\mu''$  are associated with the magnetic properties [35].

From Eq. (1) and (2)

$$d = d' + jd'' = \frac{c}{2\pi\sqrt{\mu^*\varepsilon^*}} \arctan\left(-j\sqrt{\frac{\mu^*}{\varepsilon^*}}\right) \quad (3)$$

Then, Eq. (3) was used to calculate the dependence of the complex parameter  $d$  on the frequency  $f$  and to find the minima of the ratio  $\left|\frac{d''}{d}\right|$  from the obtained curve. Then, the minima for which  $\left|\frac{d''}{d}\right| \leq 0.01$  are selected and the thicknesses  $d_0 = d'$  corresponding to these minima are determined. For the selected values of the parameter  $d_0$ , the frequency characteristics of the reflection loss are calculated with Eq. (1) and (2).

The electromagnetic waves at higher frequencies penetrate only near the surface of the conducting shield, and the magnitude of the field exponentially decays with thickness. The distance (i.e., the thickness of the shield) required for the electromagnetic wave to be diminished to  $1/e$  or 37% is known as the skin depth ( $\delta$ ), which can be mathematically expressed by Eq. 4 [36].

$$\delta = \sqrt{\frac{1}{\pi f \sigma \mu}} \quad (4)$$

in which,  $\mu$  – magnetic permeability,  $\mu = \mu_0 \cdot \mu_r$ , where  $\mu_r$  is the relative permeability,  $\mu_0$  – permeability of free space ( $\mu_0 = 4\pi 10^{-7}$  H/m),  $\sigma = \omega \varepsilon_0 \varepsilon''$  is the AC conductivity and  $f$  is the frequency [37].

### 1.5.2 Calculation of shielding effectiveness

The electromagnetic interference shielding refers to the attenuation of the transmitting electromagnetic waves by the shielding material. A high value of electromagnetic interference (EMI) shielding effectiveness (SE) means less energy transmitted through the shielding material. For commercial applications, a shielding material that possesses the (SE) of 20 dB can block 99% of the incident electromagnetic waves. The total shielding effectiveness ( $SE_T$ ) is given as:

$$SE_T(\text{dB}) = SE_R + SE_A \quad (5)$$

The shielding effectiveness can be evaluated on the basis of scattering parameters ( $S_{11}, S_{21}, S_{21}, S_{22}$ ) by the following equations (6, 7, 8):

$$SE_R = 10 \log_{10} \left( \frac{1}{1-R} \right) = 10 \log_{10} \left( \frac{1}{1-|S_{11}|^2} \right) \quad (6)$$

$$SE_A = 10 \log_{10} \left( \frac{1-R}{T} \right) = 10 \log_{10} \left( \frac{1-|S_{11}|^2}{|S_{21}|^2} \right) \quad (7)$$

$$SE_T = 10 \log_{10} \left( \frac{1}{T} \right) = 10 \log_{10} \left( \frac{1}{|S_{21}|^2} \right) \quad (8)$$

## 1.6 Measurement techniques

### 1.6.1 Dielectric and magnetic properties

Absorbing properties of composites are determined by the electrodynamics characteristics of the materials [38]. Magnetic properties of magnetic composites can be described by complex permeability ( $\mu^* = \mu' - i\mu''$ ), where  $\mu'$  is real permeability and  $\mu''$  is imaginary permeability. Both parts of  $\mu^*$  increase with concentration of magnetic filler in composite. Real permeability ( $\mu'$ ) and imaginary permeability ( $\mu''$ ) signify magnetic storage and losses, respectively. Dielectric properties are represented as  $\varepsilon^* = \varepsilon' - i\varepsilon''$ . Real permittivity ( $\varepsilon'$ ) signifies the charge storage (or dielectric constant) or electric energy storage capacity, whereas imaginary permittivity ( $\varepsilon''$ ) represents an amount of dielectric dissipation or losses [39, 40, 41].

### 1.6.2 S-parameters measurement

These techniques include free-space methods, open-ended coaxial-probe techniques, cavity resonators, dielectric-resonator techniques, and magnetic material test fixture and transmission-line techniques. Standard magnetic measurements are based on tests of standard toroids – typically using a toroidal core.

#### *Impedance method (1 MHz – 3 GHz)*

There are many measurement methods to choose from when measuring impedance, each of which has advantages and disadvantages. In measurements from 100 MHz to 3 GHz, the RF impedance method has the best measurement capability.

#### *Free-space method (2 – 20 GHz)*

The basic free space measurement system consists of: a network analyser, a sample holder, two horn antennas and software. The free-space measurement technique has the advantages of allowing reflection and transmission measurements without any physical contact with the sample. The concept of transmission and reflection FSM is shown in Fig. 6 a, b, c. After the measurement, the *S-parameters* are used for extracting the electromagnetic properties of the sample.



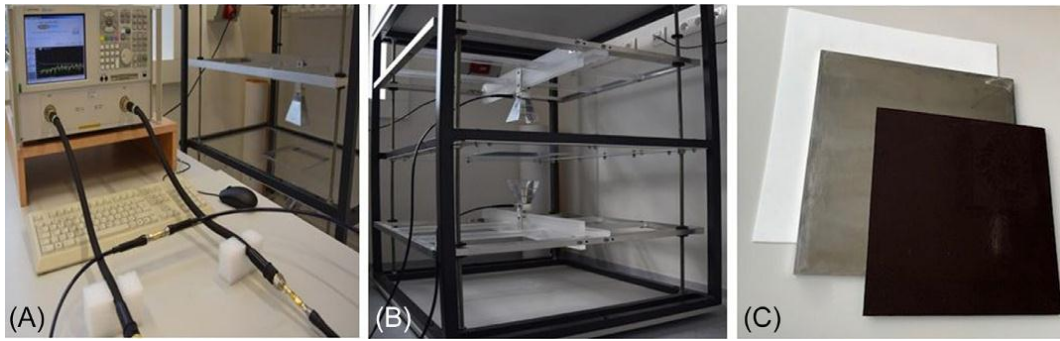


*Figure 6: Free-space measurement method a) A two-port (A) PNA-L network analyser (N5230A) b) antennas c) calibration plates.*

### *Waveguides*

Above 2 GHz, the wavelength is short enough to allow practical, efficient energy transfer by different means. A waveguide is a conducting tube through which energy is transmitted in the form of electromagnetic waves as shown in The electromagnetic fields are propagated through the waveguide by means of reflections against its inner walls, which are considered perfect conductors.

## 2. AIMS OF THE THESIS

The main aim of this work was the development of magnetic type polymer composites for EMI applications as radio absorbers (RAs) and the optimization of their mechanical properties.

To accomplish the aim, the following task was outlined:

- a) Application of magnetically soft MnZn, CI, and conductive CB and CNT fillers in ER/PDMS and NBR and TPE rubber matrices with the aim of preparing composite materials with absorption shielding effects of electromagnetic waves.
- b) Research on shielding efficiency against an electromagnetic field depending on composite parameters (matrix type, filler type, filler particle size, filler concentration, absorber thickness and operating frequency bandwidth).
- c) Study of mechanical properties of polymeric composite materials with an epoxy or elastomeric matrix and electromagnetic filler (MnZn, CI, CB, CNT).
- d) The calculations of reflection loss RL (dB) of single-layer metal-backed RAs were carried out on the basis of the electromagnetic properties of the composites in the RF band using the impedance method (1 MHz – 3 GHz for ER/PDMS and NBR composites and 1 MHz – 18 GHz for TPE composites).

### 3. EXPERIMENTAL SECTION

#### 3.1 Materials

Sintered MnZn ferrite is a commercially available sintered ferrite produced by Ferroprigor, Russian Federation) with high initial permeability ( $\mu_i = 3000 - 5000$ ), a maximum magnetic permeability of  $\mu_{max} \sim 3700-5200$ , a conductivity of  $\sigma_f = 2 \times 10^{-2}$  S/m, and a density of  $\rho_f = 4.8$  g/cm<sup>3</sup> [39, 42, 43]. Carbonyl irons (CI) are highly pure spherical iron particles ( $\pm 98\%$  Fe). CI was soft grade SL from company BASF with a diameter  $d_{50} = 5$   $\mu$ m. The epoxy resin used was a bisphenol A diglycidyl ether (DGEBA, D-3415, epoxide equivalent weight = 172 – 176 g, liquid, Sigma Aldrich, USA). The curing agent was an aliphatic amine, diethylenetriamine (DETA-D93856, Sigma Aldrich, USA). Dicumyl peroxide (DCP, Sigma Aldrich, USA) was used as a free radical initiator. Vinyl terminated polydimethylsiloxane (PDMS-VT) (Sigma Aldrich, USA). Propylene-based thermoplastic elastomer (TPE), trade name Vistamaxx™ 6202 (ExxonMobil, USA) is primarily composed of isotactic propylene (85 wt. %) repeat units with random ethylene (15 wt. %) distribution produced using metallocene catalyst technology (melt flow index of 7.4 g/10 min, with a density of 0.861 g cm<sup>-3</sup>, 190 °C). The main characteristics of the fillers and matrix are presented in Tab. 1 and 2. Acrylonitrile-butadiene rubber (NBR), type SKN 3345, acrylonitrile content 31 – 33%,  $\rho = 0.94$  g/cm<sup>3</sup> was supplied from Sibur, Russia Federation. Multi-walled CNT (type NC7000, content of carbon 90%, length of tubes is 1.5  $\mu$ m, diameter of tubes 9.5 nm, specific surface area 250 – 300 m<sup>2</sup>/g) was provided from Nanocyl SA, Sambreville, Belgium. CB (type Vulcan XC72) was compounded in Vipo, a.s. Partizánske, Slovakia. A standard sulphur-based curing system consisting of activators zinc oxide and stearic acid (Slovlak, Košeca, Slovakia), accelerator N-cyclohexyl-2-benzothiazole sulfenamide (Duslo, Šal'a, Slovakia) and sulphur (Siarkopol, Tarnobrzeg, Poland) was used for cross-linking of composites.

Table 1: Physical-mechanical properties of selected matrix

Type of matrix	Vinyl-terminated polydimethylsiloxane	TPE
Tensile strength, MPa	0.4	5.5
Elongation at break, %	98	2000
Working temperature, °C	-50/153	-30/130
Specific gravity, g/cm <sup>3</sup>	0.965	0.862
Viscosity at 25°C, mPa·s	850 - 1150	1137

Table 2: Basic properties of fillers

Filler	Diameter of particles $\mu\text{m}$	Purity %	Density $\text{g}/\text{cm}^3$
MnZn	45 – 50	99.5	4.8
CI	5	99.5	7.9
CB	0.05	99.5	1.8
CNT	0.03	99.5	1.74

According to the SEM image (Fig. 7a); polycrystalline particles of MnZn ferrite consist of separate grains in the form of polyhedrons with clear-cut boundaries. The CI particles are spherical and varying in size within a few microns in diameter; herewith, a significant part of the particles form irregularly-shaped aggregates (Fig. 7b).

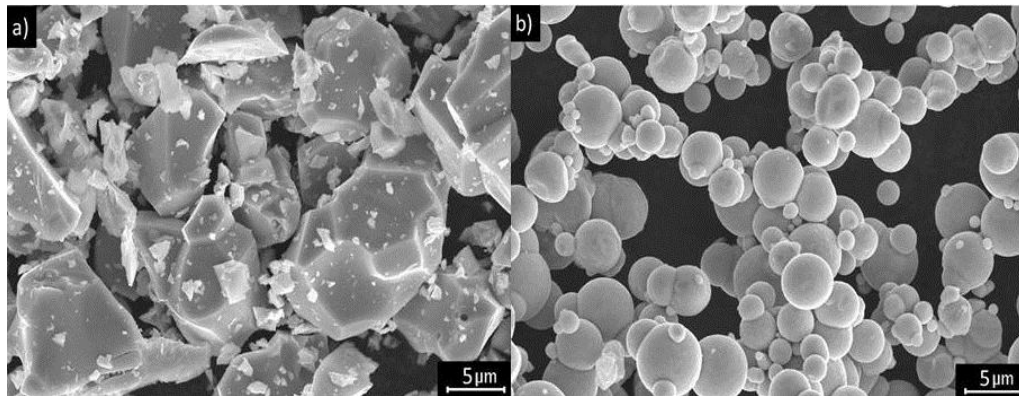


Figure 7: The SEM micrographs of the magnetic filler: a) MnZn ferrite b) CI

## 3.2 Sample preparation

### 3.2.1 Polymer blend preparation

An immiscible polymer blend of DGEBA, PDMS (10-30 wt.%) and DCP (0.5 wt.%) was prepared under mechanical stirring (MM-1000, Biosan, Germany) at 300 rpm under a nitrogen atmosphere for 2 hours at 130 °C. This mixing procedure resulted in improvement of the interphase between PDMS and the ER phase, leading to spherical particles and the cross-linking of PDMS.

### 3.2.2 Fabrication of the ER/PDMS/MnZn and ER/PDMS/CI blends

The obtained blend was loaded with magnetic filler (CI or MnZn ferrite) and stirred at 80 °C for 30 minutes. The concentration of the filler in the blend varied from 50 wt. % up to 80 wt. %. An equimolar amount of DETA curing agent was added to the mixture after 10 minutes before casting the composition into a mold

preheated to 70°C. The curing process was performed at 100 °C for 30 minutes and 1 hour at 140 °C. A relaxation process was carried out for 6 h at 60 °C.

### **3.2.3 Preparation of the NBR/MnZn, NBR/CB and NBR/CNT elastomer composites**

The amounts of curing additives were kept constant in all rubber compounds and there was a change only in the type and amount of the filler. MnZn ferrite in a concentration scale ranging from 100 (48 wt.%) to 500 phr (82 wt.%) was used as filler in the first type of composites (NBR/MnZn). CB was incorporated in the second type (NBR/CB) of composites in the amount ranging from 2.5 phr (2.3 wt.%) to 25 phr (19 wt.%). In the third composite types, the content of CB was kept at constant levels 20 phr and the amount of MnZn ferrite was changed from 100 to 500 phr (44 wt.% – 80 wt.%).

The compounding of additives was carried out in two steps using an industrial kneading machine Buzuluk (Buzuluk Inc., Komárov, Czech Republic) and a laboratory kneading equipment Brabender (Brabender GmbH & Co. KG, Duisburg, Germany). The speed of the rotor was set up to 50 rpm and the kneading chamber was heated to 90 °C [44].

In the case of composites filled with ferrite and CB NBR was first plasticised for 2.5 min. Subsequently activators were added, and after the next two 2 minutes, filler was applied. The total time of the first step mixing was 9 min at 90 °C and 50 rpm. In the second step (4 min, 90 °C, 50 rpm), the accelerator N-cyclohexyl 22benzothiazole sulfenamide (CBS) and sulphur were introduced.

### **3.2.4 Preparation of the TPE/MnZn and TPE/CI composites**

The homogeneous TPE polymer composites filled with MnZn and CI particles were prepared by mixing both components. The compound was mixed using a micro-compounder (MC5, Xplore Instruments BV, Sittard, The Netherlands). The melt mixing conditions were 190 °C for 7 minutes at 150 rpm. Before melt mixing, TPE and fillers were dried in a vacuum oven at 90 °C for 12 h. The TPE-based composites containing (50 wt. %, 70 wt. %, 80 wt. %) MnZn and CI fillers were studied.

## **3.3 Characterization techniques**

### *Scanning electron microscopy*

To investigate the phase morphology of the epoxy-polydimethylsiloxane/magnetic composites, a VEGA/LMU Tescan scanning electron microscopy (SEM) was used. The SEM images were obtained under conventional secondary electron imaging conditions with an acceleration voltage of 25 kV and a resolution of 3 nm at 30 kV.

### *X-ray photoelectron spectroscopy (XPS)*

The X-ray photoelectron spectroscopy (XPS) signals were recorded using a Thermo Scientific K-AlphaXPS system (Thermo Fisher Scientific, UK) equipped with a micro-focused monochromatic Al K $\alpha$  X-ray source (1486.68 eV). An X-ray beam of 400  $\mu$ m in size was used at 6 mA and 12 kV. The spectra were acquired in the constant analyser energy mode with pass energy of 200 eV for the survey. The narrow regions were collected with pass energy of 50 eV.

### *DC conductivity*

The DC conductivity was measured by a four-point van der Pauw method (Keithley 6517A, USA) with a current meter and a Multimeter (Keithley 2410, USA) as a source.

### *Magnetic and dielectric spectra*

The electromagnetic properties of the composites ( $\epsilon^*$  and  $\mu^*$ ) in an RF range from 1 MHz to 3 GHz were measured by the impedance method using (Impedance/Material Analyser E4991A, Agilent Technologies USA). The dielectric spectra were measured on the circular samples with a diameter of 15 mm and the magnetic spectra were measured on the toroidal samples with an outer diameter of 8 mm and an inner diameter of 3.1 mm and 2 mm thickness.

### *Dynamical mechanical analysis*

The dynamical mechanical analysis (DMA) were carried out under dual cantilever geometry in dynamic (frequency/strain experiments) on a Mettler Toledo DMA1 dynamic mechanical thermal analyser (DMTA) equipped with a liquid-nitrogen apparatus operating in a three-point bending mode. The tested samples had a dimension of 35 $\times$ 10 $\times$ 3 mm. The dynamic analysis was carried out from -120  $^{\circ}$ C to 180  $^{\circ}$ C at a heating rate of 3  $^{\circ}$ C/min, with a fixed frequency of 1 Hz and an amplitude of 20  $\mu$ m.

### *Charpy impact tests*

The Charpy impact tests were performed in accordance with ISO 179 on unnotched izod specimens using an impact tester (Zwick/Roell, Germany). The dimensions of the samples were 35 $\times$ 10 $\times$ 3 mm. The fracture mechanism of the polymer systems was studied on the surface of the fractured area via SEM. The mean values over five specimens are presented.

### *Tensile tests*

The tensile properties of composites were evaluated by using Zwick Roell/Z 2.5 appliance (Zwick Roell Group, Ulm, Germany). The cross-head speed of the measuring device was set up to 500 mm/min and the tests were carried out in compliance with the valid technical standards. Dumbbell-shaped test specimens (thickness 2 mm, length 80 mm, width 6.4 mm) were used for measurements.

## 4. RESULTS AND DISCUSSION

### 4.1 Morphology

#### 4.1.1 The ER/PDMS/MnZn and ER/PDMS/CI composites

The SEM images of the polymer matrixes and the magnetic composites on their base are shown in Fig. 10. The neat ER shows a smooth fracture surface at the brittle failure (Fig. 8a, b). The epoxy resin modified by PDMS (10 – 30 wt. %) exhibits a two-phase microstructure consisting of spherical elastomeric particles (15-90  $\mu\text{m}$ ) uniformly distributed in the bulk of the ER (Fig. 10c, d). An increase in the filler content to 70 – 80 wt. % leads to the formation of particle clusters both in the bulk of the composite and at the ER-PDMS-interface (Fig. 8c, d).

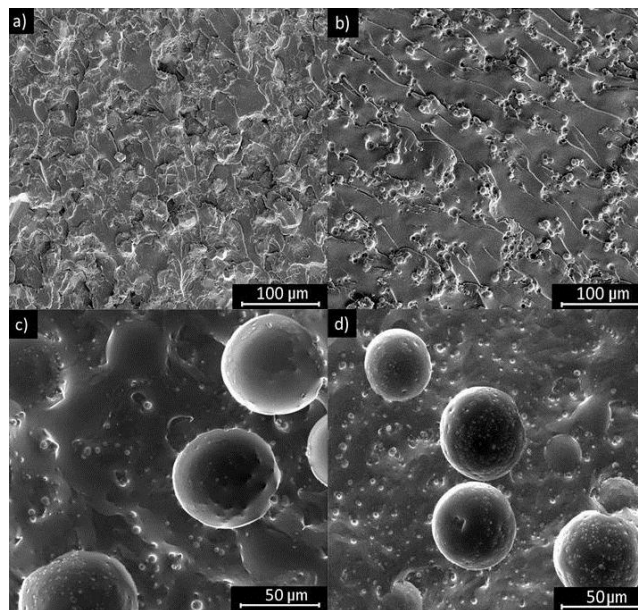


*Figure 8: The SEM micrographs of the composites: a) ER/MnZn50 b) ER/CI50 c) ER/PDMS10/CI70 d) ER/PDMS10/CI80*

#### 4.1.2 The NBR/MnZn composites

On Fig. 9a SEM images with a magnification of 100x show the distribution of the filler in the used matrix. The best distribution and dispersion of the filler could be observed in the case of NBR-based composites with 500 phr (82 wt. %) of MnZn, precisely because of the high viscosity of the given rubber mixture. In addition, in terms of chemical structure, MnZn ferrite belongs among polar materials, therefore the assumption of mutual adhesion and compatibility with the partially polar rubber matrix (NBR) [44, 45].

#### 4.1.3 The NBR/CB/MnZn composites

The morphology of the fracture surfaces of composites filled with a combination of carbon fillers and MnZn is shown in the SEM images in Fig. 9b. In general, the larger the particles, the smaller their specific surface area and the lower the effective reactive sites for interactions with rubber chains. Lower

adhesion and weaker interactions between the MnZn and the rubber matrix caused the mechanical properties of the hybrid composites to deteriorate with increasing amounts of MnZn.

#### 4.1.4 The NBR/CB and NBR/CNT composites

A SEM analysis of the fracture surfaces of the composites confirmed that better dispersion, homogeneity and mutual adhesion between the carbon-based fillers and the elastomeric matrix were achieved for composites filled with CNT. The reason for the better adhesion between the CNT particles and the rubber matrix can be attributed to the larger specific surface area of the CNT and the strong physical or physicochemical interactions between the two components [46].

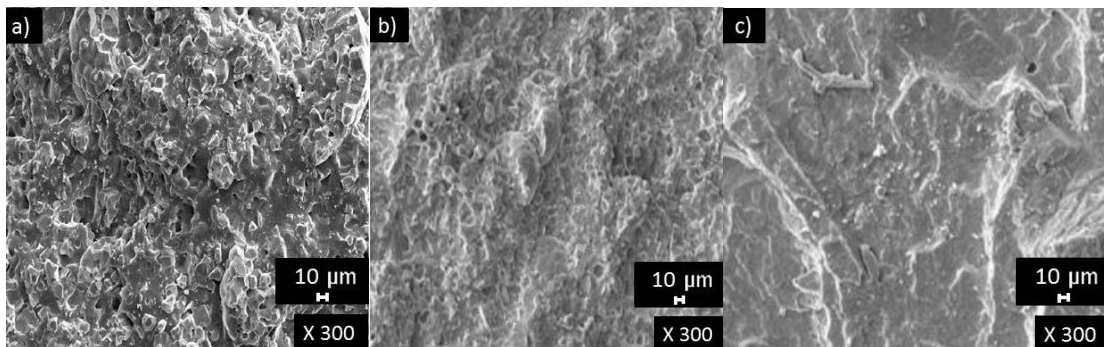


Figure 9: SEM images of NBR composite a) filled with 500 phr of MnZn, b) NBR composites based on 20 phr CB and 300 phr MnZn, c) NBR composites based on 20 phr CB

#### 4.1.5 The TPE/MnZn and TPE/CI composites

SEM images (Fig. 10a, b) with a magnification of 100x show the distribution of the filler in the used matrix. In addition, it is also possible to notice small defects, which were probably created by freezing the samples below the glass transition temperature and their subsequent breaking in order to obtain fracture surfaces for microscopic analysis. On the other hand, the distribution and dispersion of the MnZn and CI magnetic filler is better, which can be attributed to the higher viscosity of the TPE-based mixtures.

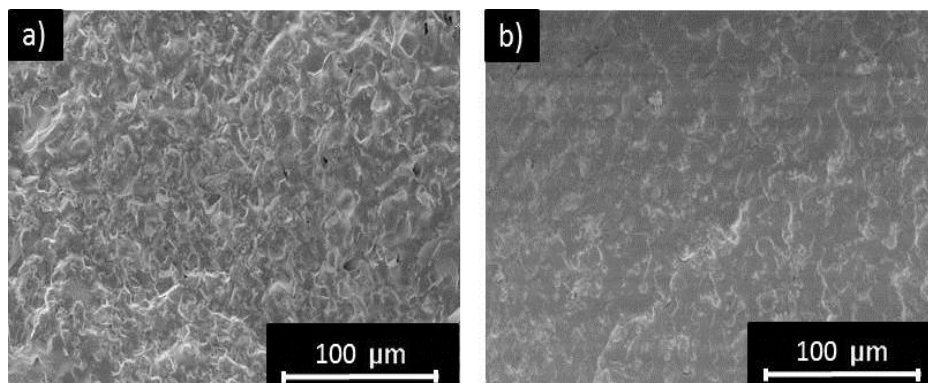


Figure 10: SEM images of fracture surfaces of TPE composites based on 70 wt. % of a) MnZn and b) CI



## 4.2 Dielectric and magnetic properties

### 4.2.1 The complex permittivity of ER/PDMS composites

The composites with MnZn ferrite show a frequency dispersion of  $\epsilon^*$  in the entire investigated frequency range, and it is more pronounced for the highly-filled composites. The  $\epsilon'$  and  $\epsilon''$  values gradually increase with the filler content (Fig. 11). The effect of the polymer matrix composition on the complex permittivity appeared for the composites with 70 – 80 wt. % of filler. Thus, the ER/PDMS-MnZn composites show higher values of  $\epsilon'$  and  $\epsilon''$  compared with the ER composites with the same filler concentration. As to the composites with CI, the frequency dispersion of the complex permittivity is less pronounced compared to the composites with MnZn, but  $\epsilon'$  and  $\epsilon''$  are increasing with the filler concentration to approximately the same level as in the composites with MnZn ferrite. It seems that the permittivity spectra of the composites is caused by the electrical polarization induced in the filler particles and the particle clusters.

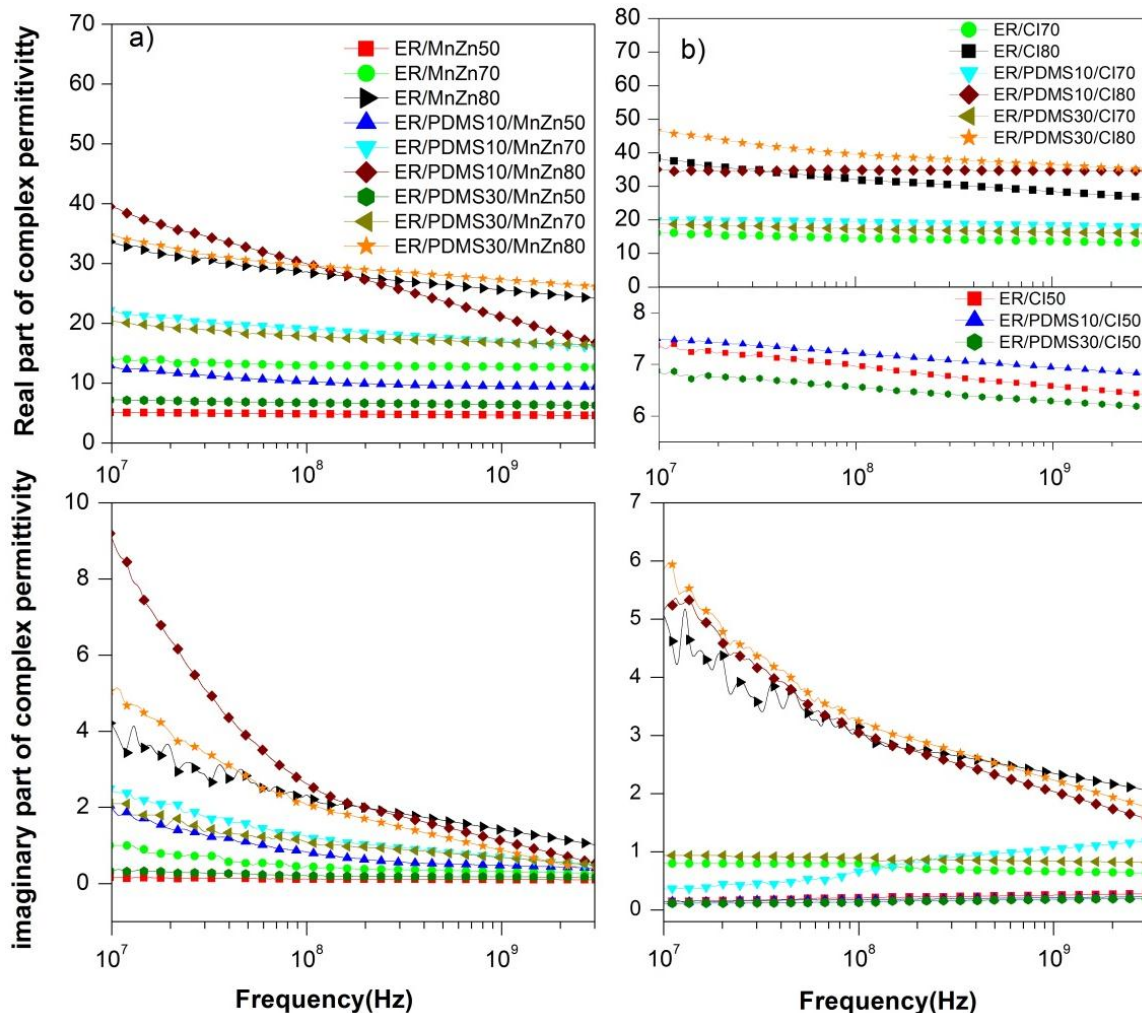


Figure 11: The frequency dependences of the complex permittivity of the polymer composites filled with a) MnZn and b) CI (wt. %) [49]

#### 4.2.2 The complex permittivity of NBR/MnZn and hybrid NBR/CB/MnZn composites

The frequency dependencies of real  $\epsilon'$  and imaginary  $\epsilon''$  parts of complex (relative) permittivity  $\epsilon = \epsilon' - j \epsilon''$  for the composite materials are graphically illustrated in Fig. 12 a. It becomes obvious that the real part  $\epsilon'$  steeply decreases at frequencies up to about 10 MHz, then settles on a constant value. It can also be seen that with increasing content of MnZn in composites, the real permittivity shifts to higher values. When the amount of magnetic filler increased from 100 to 500 phr (48 – 82 wt. %), the real permittivity increased from 18.2 to 73.8. The achieved changes in frequency dependencies of complex permittivity may be attributed to various types of polarization mechanisms originating in the filler [44]. As seen at Fig. 12 b, after sharp decrease of  $\epsilon'$  at frequencies up to about 10 MHz, it fluctuates in a low range of experimental values. The lowest  $\epsilon'$  was found to have the composite filled with 20 phr (16 wt. %) of CB ( $\epsilon' = 30$  at 1 MHz). By increasing frequency up to 3 GHz, it decreased to 7. The real permittivity of the hybrid composite filled with 20 phr (8.7 wt.%) of CB and 100 phr (44 wt.%) of MnZn decreased from 47 down to 12 when the electromagnetic radiation frequency increased from 1 MHz to 3 GHz. The increase in magnetic filler content to 500 phr (80 wt. %) resulted in the increase of real permittivity up to almost 132 at 1 MHz. The initial decrease of real permittivity with frequency may be attributed to the semiconductive character of MnZn ferrite and conductive character of CB. The increasing amount of filler loading results in the increase of both, real and imaginary permittivity [47, 48].

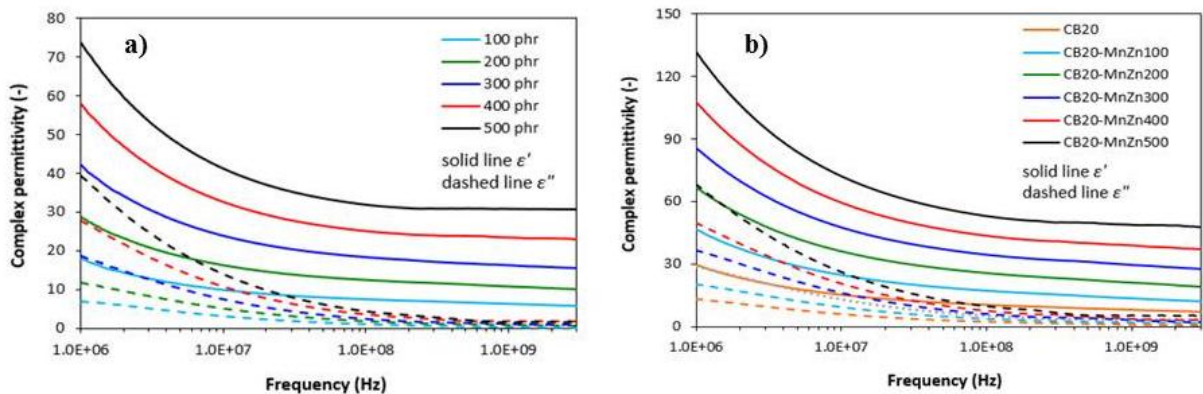


Figure 12: Frequency dependences of real  $\epsilon'$  and imaginary  $\epsilon''$  parts of complex permittivity for a) NBR composites filled with ferrite MnZn, b) hybrid NBR/CB/MnZn composites [44]

#### 4.2.3 The complex permeability of ER/PDMS composites

The frequency dependence of the  $\mu^*$  of the MnZn and CI based composites is determined first of all by the type of magnetic filler and its concentration. The permeability dispersion region for the MnZn-based composites occupy a

frequency range from  $10^6$  Hz up to  $10^9$  Hz, with a maximum value of  $\mu'=10$  and  $\mu''=3$  for 80 wt.% of filler (Fig. 13).

The CI-based composites demonstrate a similar behaviour of magnetic spectra with the difference being that the ferromagnetic resonance linewidth is broader,  $10^6 - 10^{10}$  Hz. However, the absolute value of the  $\mu^*$  is lower compared to the composites filled with MnZn ferrite due to the skin effect, which masks the magnetization processes in the conductive CI particles. Besides, there are two peaks on  $\mu''(f)$  for the composites with 50–80 wt. % of CI at about  $10^8$  Hz. (domain-wall resonance) and  $4 \times 10^9$  Hz (spin resonance) [49].

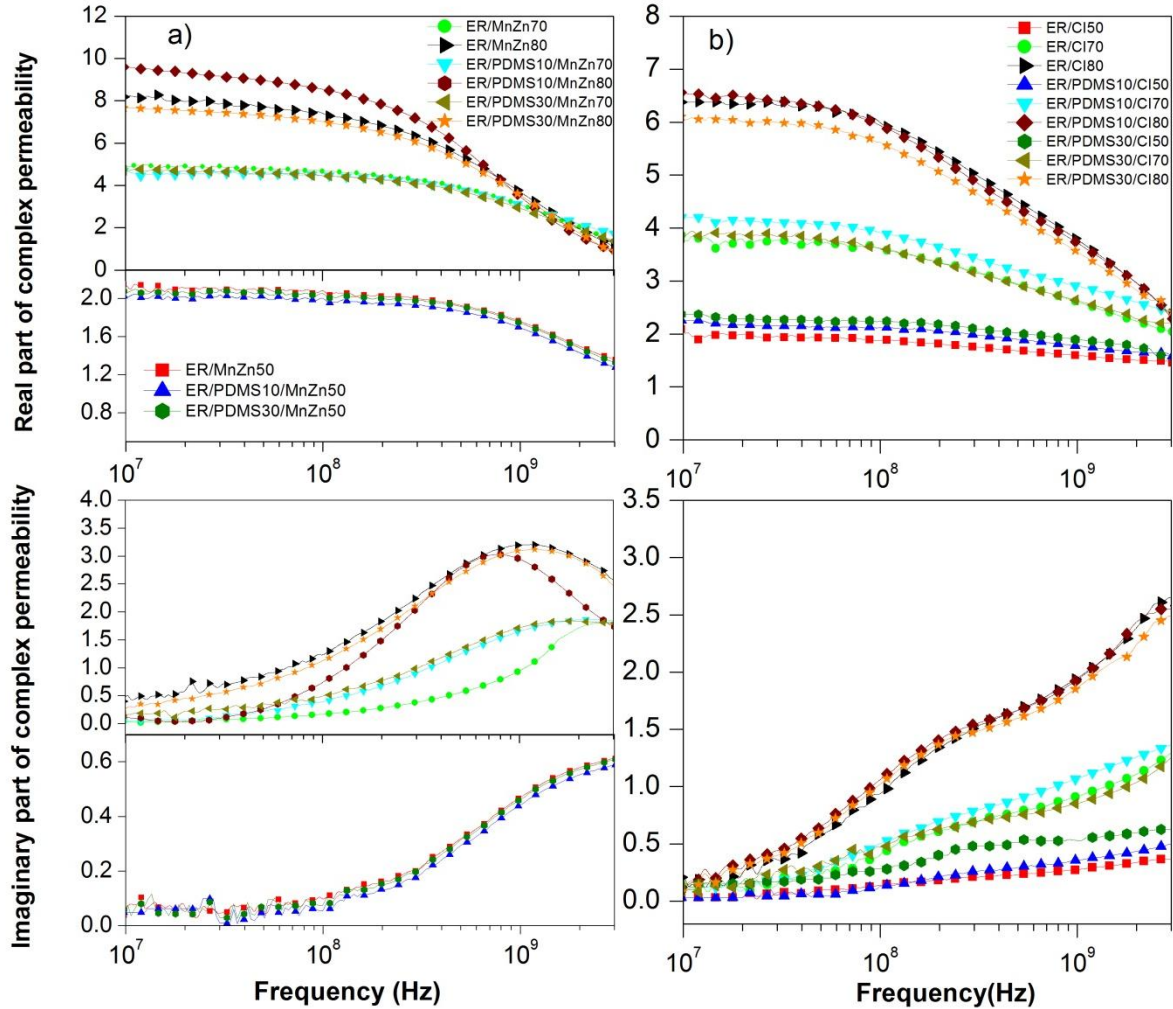


Figure 13: The frequency dependence of the complex magnetic permeability of the polymer composites filled with a) MnZn and b) CI (wt. %) [49]

According to the magnetic spectra, the demagnetizing field in the composites with all types of the matrix approaches a minimum at 80 wt. % (45 vol. %) of MnZn and CI. The SEM images of the highly-filled composites indicate the formation of particle clusters as in the volume of the composite as on the ER/PDMS interface (Fig. 8 c, d). As the particles make a chain, demagnetization decreases due to a decrease in the magnetic poles number and the formation of the continuities magnetization flux lines (Fig. 14).

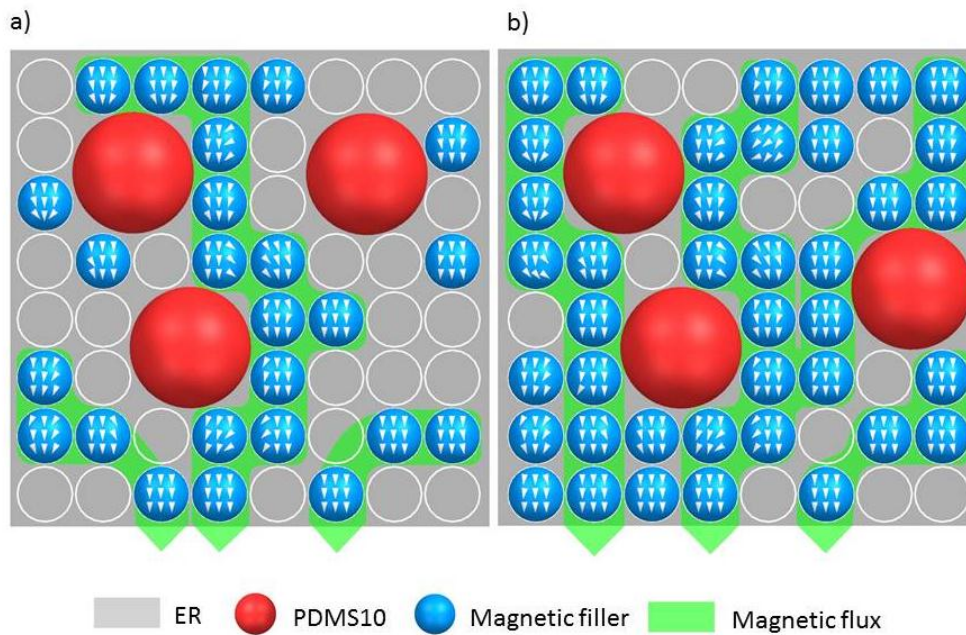


Figure 14: The effect of the filler concentration on the field internal demagnetizing in the magnetic composites: a) 50 wt. % magnetic filler  
b) 70 wt. % magnetic filler [49]

#### 4.2.4 The complex permeability of NBR/MnZn and NBR/CB/MnZn composites

The frequency dependencies of real and imaginary parts of complex permeability ( $\mu = \mu' - j\mu''$ ) for rubber magnetic composites are presented in Fig. 15 a. As shown, there is only small change of the real part  $\mu'$  with the change in frequency up to about 200 MHz, and then it decreases close to one. The imaginary permeability  $\mu''$  can be neglected up to about 100 MHz, then increases and after reaching a maximum at a resonance frequency  $f_r$ , it drops down to a low value. It also becomes apparent from Fig. 15 that the real permeability of composites at low frequencies increases with an increasing content of magnetic soft filler, from 3.3 for the composite filled 100 phr (48 wt. %) of MnZn ferrite, to 7.5 for the maximally filled composite at 1 MHz. The lowest real and imaginary permeability was found to have the composite filled only with CB and their values seem also to be independent on frequency (Fig. 15 b). The increasing amount of magnetic filler in hybrid composites resulted in the increase of real permeability. The addition of CB increases demagnetization field, which leads to a reduction in the permeability value of the complex [3].

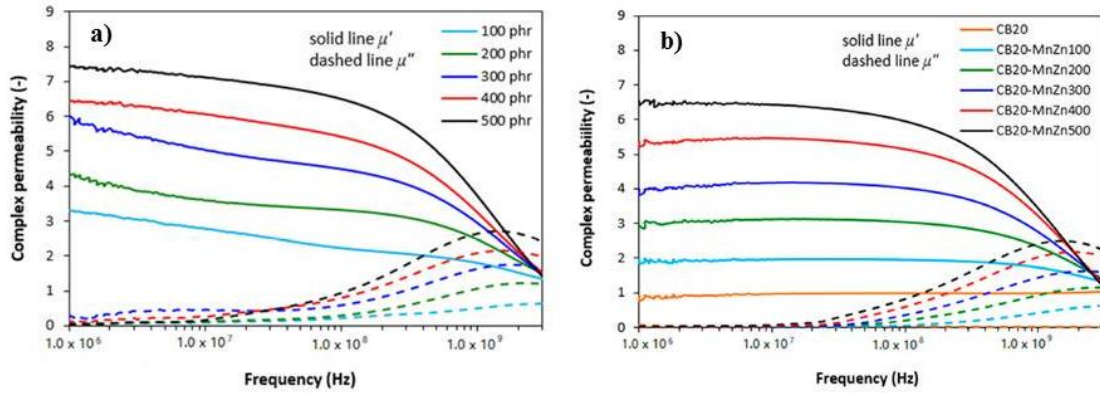


Figure 15: Frequency dependences of real  $\mu'$  and imaginary  $\mu''$  parts of complex permeability for a) MnZn filled NBR composites, b) CB20/MnZn filled NBR composites [3]

### 4.3 Electromagnetic shielding characteristics of composites

#### 4.3.1 RL of the ER/PDMS/MnZn and ER/PDMS/CI composites

In order to characterize the electromagnetic wave absorption properties of the composites obtained, the reflection minima of single-layer absorbers was calculated within the layer thickness (eq. 3). The results obtained are shown in Fig. 16. After that, the operating absorption bandwidth at the -10 dB level of RL was evaluated (eq. 9) The composites with MnZn ferrite demonstrate a larger bandwidth to thickness ratio in comparison with the CI-filled composites due to a proper ratio between  $\epsilon^*$  and  $\mu^*$ , which leads to the impedance matching conditions between the RAs and the free space. In general, it can be found that the magnetic composites based on the ER/ PDMS10 matrix achieved higher RL bandwidths than the ER and the ER/ PDMS30 composites with the same magnetic filler content [10]. Figure 16 shows the calculated RL dependence for the composites with 50 wt. % of MnZn ferrite in the ER matrix and blends with a different PDMS content. The addition of 10 wt. % of PDMS to the ER (ER/PDMS10/MnZn50) results in a higher absorption (-25 dB) within a broader bandwidth ( $\Delta\lambda/d = 6.28$ ) for an RA with a thickness of about 7 mm.

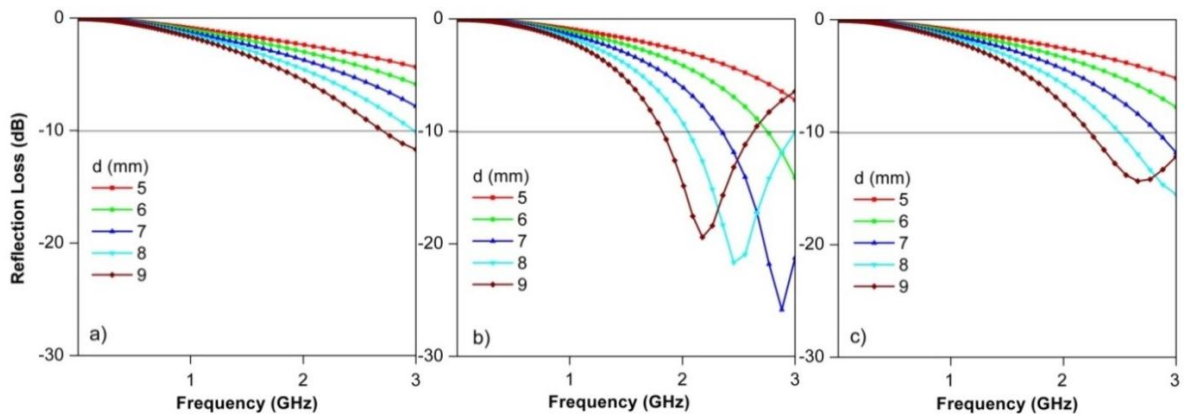


Figure 16: The frequency dependence of the reflection loss of the composites filled with 50 wt. % MnZn based on: a) ER b) ER/PDMS10 and c) ER/PDMS30

An increase in the filler concentration up to 70 wt. % (36 vol. %) provides 99% of the electromagnetic energy absorption (Fig. 17). Besides that, the magnetic composites with a different PDMS content in the ER matrix exhibit a different operating frequency range: for the MnZn-filled composites  $\Delta f = 1.6 - 3$  GHz, while for the CI-filled composites  $\Delta f = 0.7 - 1.7$  GHz. According to the results obtained, the presence of 10 wt. % PDMS in both types of composites is sufficient to reduce the demagnetization effect and to obtain broadband RAs.

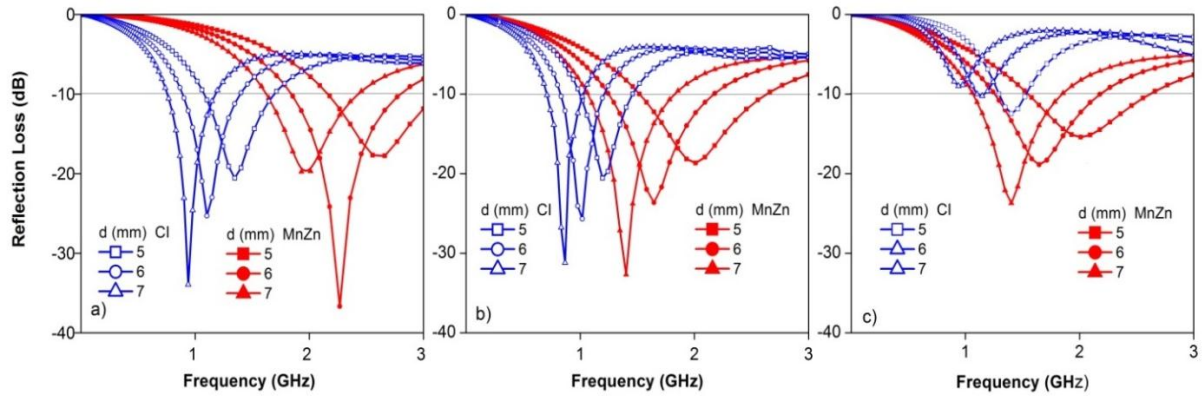


Figure 17: The frequency dependences of the reflection loss of the composites filled with MnZn (36 vol. % = 70 wt. %) and CI (36 vol. % = 80 wt. %) based on: a) ER b) ER/PDMS10 and c) ER/PDMS30 [49]

#### 4.3.2 RL of the NBR/MnZn and NBR/CB/MnZn hybrid composites

Figure 18 a) depicts the reflection loss of composites with different contents of MnZn ferrite in the operating frequency range. It is shown that all composites containing 200 phr (65 wt. %) of filler and more provide satisfactory absorption shielding efficiency. The composite containing 200 phr (65 wt.%) of MnZn exhibited reflection loss at -10 dB and -20 dB in the widest frequency range, i.e., from 1.5 GHz to 2.7 GHz at -10 dB. The absorption maximum of this composite shield is at -48 dB at a frequency of 2 GHz [44]. As the best absorption shield can be considered the hybrid CB/MnZn composite (Fig. 18 b) filled with 100 phr (44 wt. %) of MnZn as this shield exhibited return loss at -10 dB in the widest frequency bandwidth, i.e., from 1.6 to 2.35 GHz. The absorption maximum was detected at -48 dB [3].

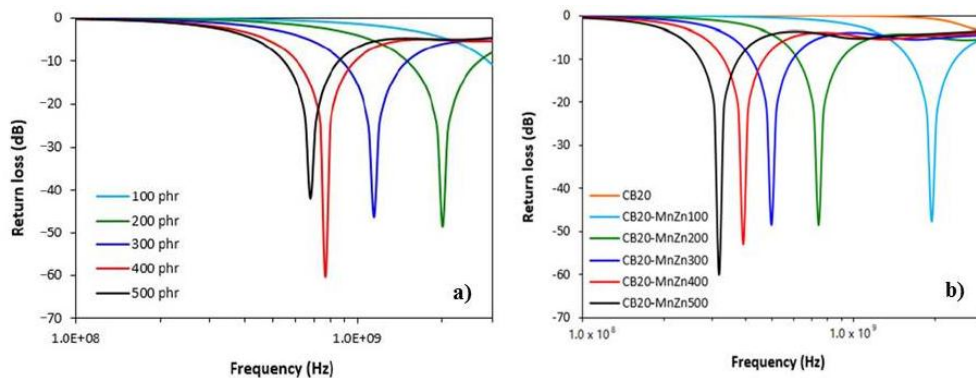


Figure 18: Frequency dependences of RL for a) NBR composites filled with MnZn, b) hybrid CB/MnZn NBR composites [3, 44]

### 4.3.3 RL of the TPE/MnZn and TPE/CI composites

In the case of propylene-based thermoplastic elastomer (TPE) composites (Fig. 19a), which were measured in the frequency range of 1 MHz – 18 GHz, it is also clear that all composites containing 70 wt. % of MnZn filler and more show sufficient absorption shielding efficiency at -10 dB. The effective absorption band of a composite with 70 wt. % of filler at -10 dB ranges from 2.79 to 6.22 GHz. The peaks of the absorption maxima of these composites are at the level of -62 dB for the composite with 70 wt. % of filler. The composite containing 70 wt. % of CI (Fig. 19 b) can be considered the most effective absorbent shielding material because it showed reflection losses at -10 dB in the widest frequency range, from 11.6 GHz to 18 GHz at -10 dB.

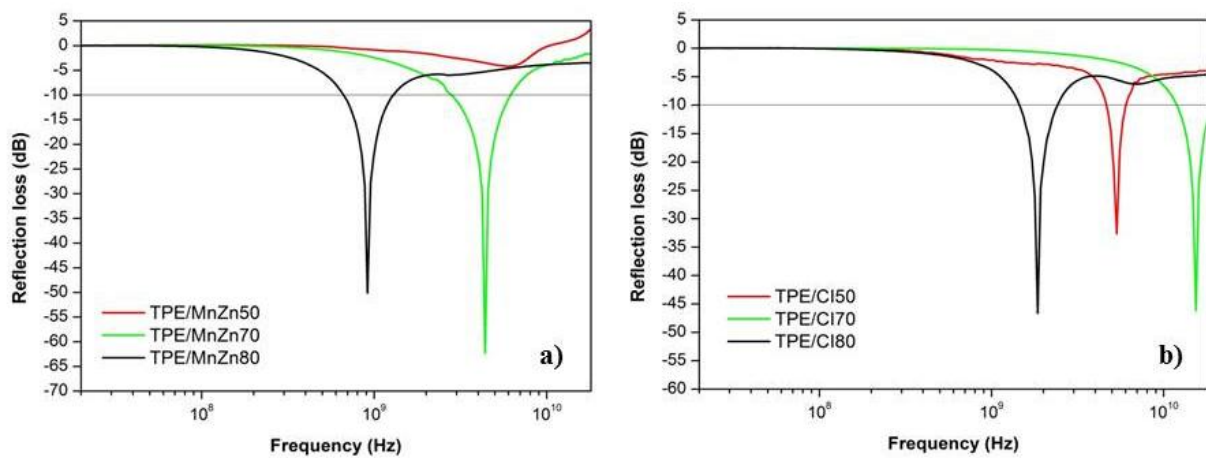


Figure 19: The frequency dependence of the reflection loss of the TPE composites filled with a) MnZn, b) CI

## 4.4 Mechanical properties

### 4.4.1 DMA of the ER/PDMS/MnZn, ER/PDMS/CI and NBR/CB composites

The polymer blend of neat epoxy resin (ER) and PDMS was studied in [50]. Figures 20 show the result of a dynamical mechanical analysis (DMA) of the magnetic composites filled with CI. The storage modulus ( $E'$ ) of the composites increases with increases in the filler concentration from 50 up to 70 wt. %. (Fig. 20a). In our study, we did not find a visible change in  $T_g$  for the composites filled with MnZn ferrite, but for a composite with CI,  $T_g$  decreases due to the filler oxidation processes, which was confirmed by the results of the XPS (Fig. 20c).

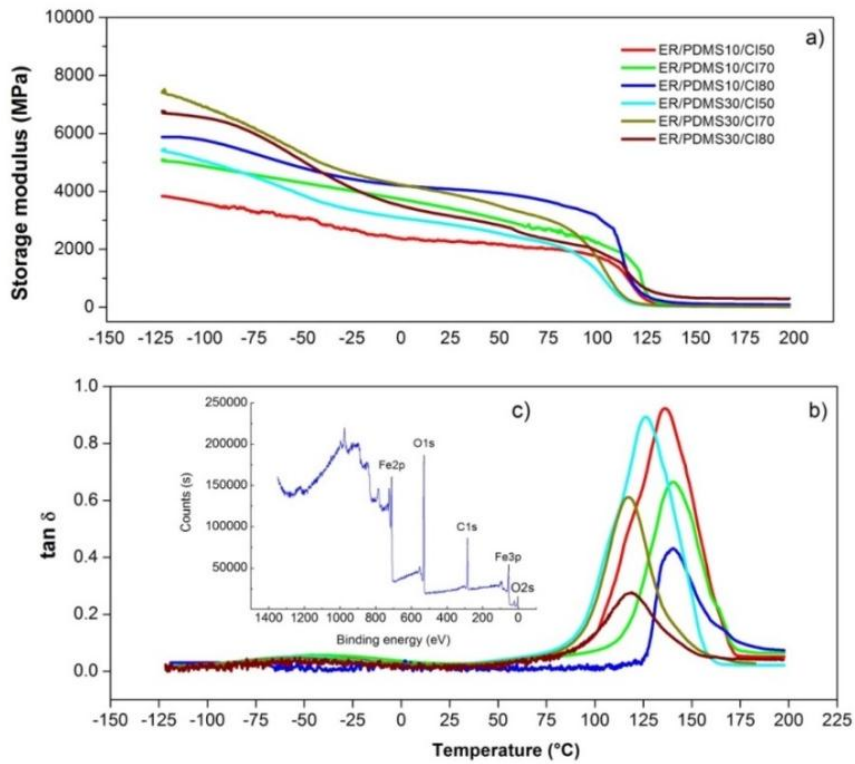


Figure 20: The temperature dependences of a) the storage modulus  $E'$  b)  $\tan \delta$  of the composite filled by CI and c) XPS of the ER/PDMS10/CI80 [49]

The peak maximum of CB/MnZn corresponds to the glass transition temperature  $T_g$  and it becomes evident that there was almost no change in  $T_g$  of CB/MnZn composites in dependence on magnetic filler content (Fig. 21). However, it should be noted that the differences in  $T_g$  of the composites were not substantial, and generally it can be stated that glass transition temperature is not significantly influenced by the composition of composites [51].

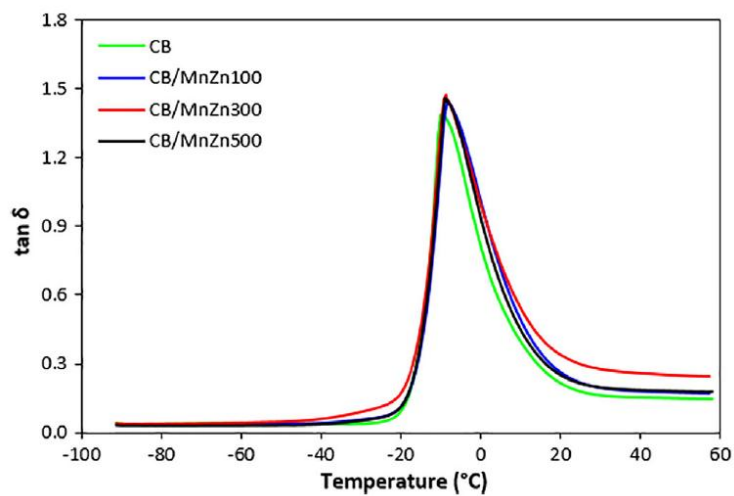


Figure 21: Temperature dependences of  $\tan \delta$  for CB/MnZn NBR composites [51]



#### 4.4.2 Tensile properties of the NBR and TPE composites

The mechanical properties of composites filled only with MnZn and hybrid composites are graphically illustrated in Fig. 22a. The highest tensile strength demonstrated the composite filled with 20 phr (8.7 wt. %) of CB and the composite filled with combination of CB and 100 phr (44 wt. %) of MnZn [3]. Dependence of the tensile strength of the TPE/MnZn and TPE/CI composites on the concentration of the magnetic fillers (Fig. 22b) shows that the highest tensile strength at break was shown by the TPE composite filled with the lowest filler content of 50 wt.% MnZn and CI as well. With a further increase in the concentration of the magnetic filler in the TPE/MnZn composites, the tensile strength shows a decreasing course of dependence.

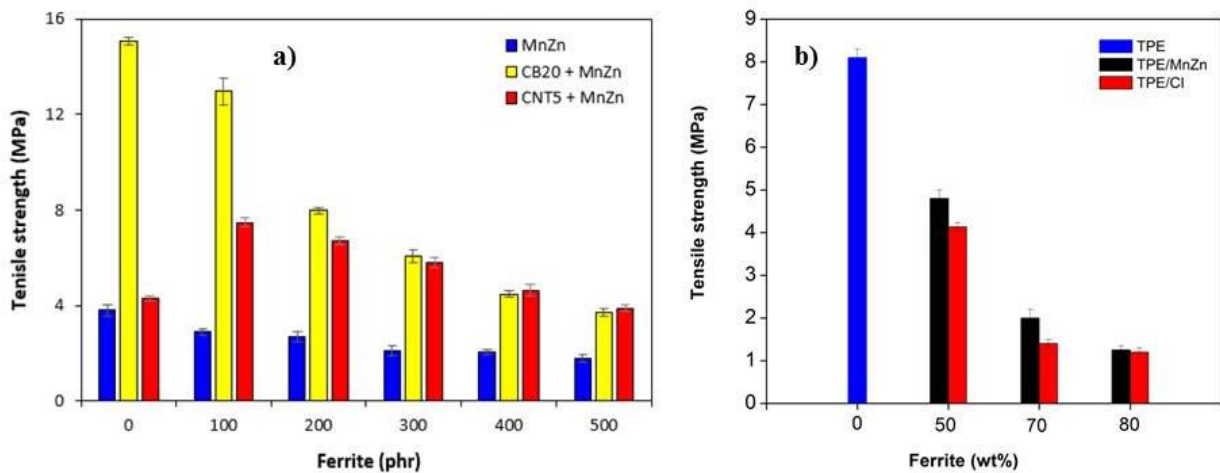


Figure 22: Tensile strength of a) hybrid NCB20/MnZn and CNT/MnZn NBR composites, b) TPE/MnZn and TPE/CI composites

#### 4.4.3 DC electrical conductivity of the ER/PDMS, NBR and TPE composites

The electrical conductivity of the pure matrix is around  $10^{-10}$  S/m. The MnZn conductivity  $\sigma_f = 2$  S/m was determined by four-point method. In the case of composites (matrix+filler) their electrical conductivity exhibits an increase (Fig. 23a). Compared to composites with 50 wt. % of MnZn, the electrical conductivity of maximally filled composites has approximately 1 orders of magnitude higher value than composites with 50 wt. % of magnetic filler. With an increase in MnZn content from 70 to 80 wt.% there was an increase in conductivity by 2 times (from  $1.15 \times 10^{-6}$  S/m for a composite filled with 70 wt.% of MnZn to  $2.7 \times 10^{-6}$  S/m for a maximum filled composite). Percolation was not clearly achieved, as composites were prepared only with a high concentration (50 - 80 wt. %) where the conductivity of the MnZn filler reached the value ( $2 \times 10^{-2}$  S/m) [42]. In the case of a TPE composite (Fig. 23b), we can observe that the conductivity for concentrations of 70 wt. % increases by 1 order for TPE/CI and by 3 order for TPE/MnZn. As the concentration increases up to 80 wt. %, the conductivity increases by 1 order for both types of fillers.

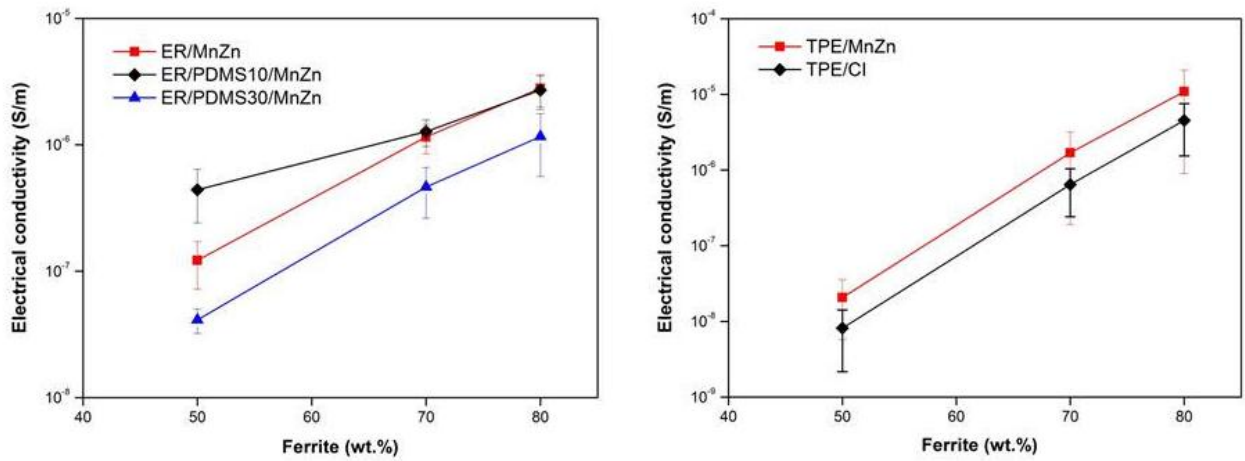


Figure 23: The concentration dependence of DC electrical conductivity on a) ER/MnZn and ER/PDMS/MnZn composites, b) TPE/MnZn and TPE/CI composites

The electrical conductivity of composites filled with MnZn ferrite and hybrid composites is depicted in Fig. 24. Composites filled with a combination of MnZn and carbon-based fillers exhibit higher electrical conductivity compared to equivalent composites filled only with MnZn ferrite. The incorporation of 100 phr (45 wt. %) magnetic filler resulted in a significant increase of electrical conductivity of hybrid CNT/MnZn composites. It is obvious that by combination of CNT and a magnetic filler, the percolation threshold and formation of conductive filler paths are reached even at low magnetic filler content, resulting in outstanding increase of electrical conductivity [3].

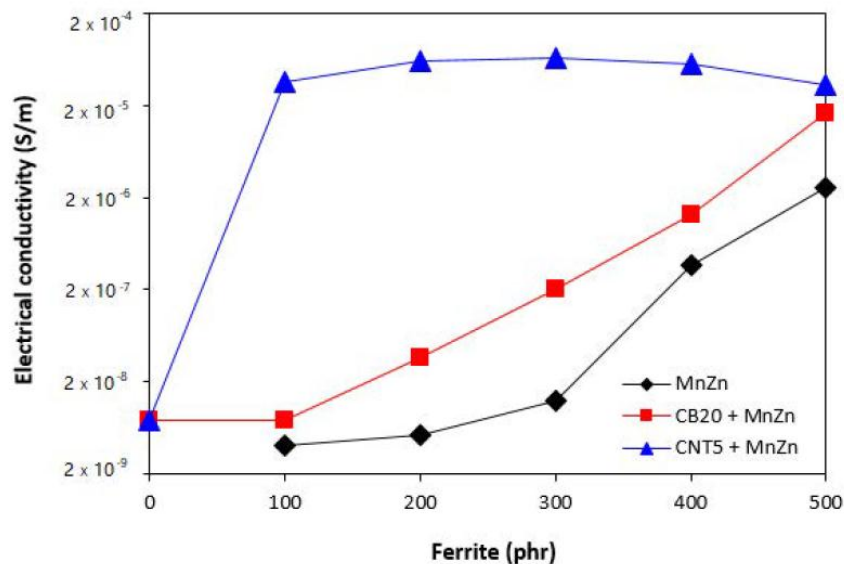


Figure 24: The concentration dependence of DC electrical conductivity on NBR/MnZn and hybrid NBR/CB20/MnZn, NMR/CNT5/MnZn composites [3]

## SUMMARY OF THE RESULTS

A dual-phase polymer matrix (ER and PDMS) filled with MnZn-ferrite and CI was investigated with the aim of optimizing the electromagnetic properties of the composites in the RF range (1 MHz – 3 GHz), as well as their mechanical properties and price. To meet this goal, the concentration of PDMS was varied from 10 to 30 wt. % which affects the distribution of the magnetic particles in the polymer matrix leading to locally-increased filler concentration in the ER phase. The SEM results showed that the filler is localized inside the ER phase and at the ER-PDMS-interface with good homogeneity. An analysis of the obtained results showed that the position of the RL minima moves to a lower frequency and the loss factors of the composites increase along with increasing the filler concentration. It has been shown that, via a selection of the matrix (ER, ER/PDMS), it is possible to change the distribution of the filler thereby significantly lowering the reflection loss. Overall, the presence of 10 wt. % PDMS in both types of composites is sufficient to reduce the demagnetization effect and to obtain broadband RAs with a thickness of 5 – 7 mm.

Hybrid elastomeric (NBR) composites showed that the permeability of MnZn and its combination with carbon fillers (CB and CNT) was dependent only on the content of magnetic filler (from 48 – 82 wt. %), regardless of the type and concentration of carbon filler. The electrical conductivity and permittivity of the composites increased in the order: NBR/MnZn composites < NBR/CB/MnZn composites < NBR/CNT/ MnZn composites ( $\sigma=3 \times 10^{-9}$  S/m,  $3 \times 10^{-8}$  S/m and  $5 \times 10^{-4}$  S/m;  $\varepsilon' = 74, 130$  and  $1008$ ). On the other hand, it reduced the absorption shielding ability of the composites in the same order (RL = -60 dB, -53 dB, -3 dB, -2.3 dB). The tensile strength decreases in the order: < CB/MnZn composites < CNT/MnZn composites < MnZn composites. At the same time, the tensile strength decreases with an increasing amount of MnZn filler. The most significant decrease is for CB/MnZn composites (from 15 – 4.2 MPa). The application of carbon-based filler led to the strengthening of the rubber matrix, better dispersion and distribution of MnZn ferrite, and subsequently to the improvement of the mechanical properties of the composites. The tensile strength increased from 3.3 MPa for the NBR/MnZn composite to 13.5 MPa for the NBR/CB20/MnZn composite (MnZn 48% by weight). The conductive CB contributed to the charge storage and various polarization mechanisms, which was manifested by an increase in real and imaginary permittivity. This was subsequently reflected in the change of absorption peaks. The MnZn-filled composite containing 200 phr (65% wt %) of magnetic filler can be considered the best absorption shielding material among all tested composites, as it demonstrated the largest absorption frequency bandwidth ( $\Delta f = 1220$  MHz) for reflection loss at -10 dB, which indicates absorption of 95% of EMI, respectively. The results also revealed an improvement in the mechanical properties of the hybrid NBR/CB/MnZn composites, where the tensile strength reached a value of 8.1 MPa.

TPE composites based on MnZn and CI fillers were investigated in the RF region (1 MHz – 18 GHz). The results show that the shielding ability of the TPE/MnZn composite occurs in the frequency band (907 MHz – 4.3 GHz) and shifts to lower frequencies with increasing concentration. The measured values show that the best absorption in the widest frequency range was achieved by the TPE/MnZn70 composite (RL = -62 dB and  $\Delta f = 3.37$  GHz). The TPE/CI70 composite achieves absorption in a wider frequency band (from 15.4 GHz to 18 GHz and RL = -46 dB), while  $f_{\max}$  is already outside the measuring range of the device. The tensile strength of both composites decreases with increasing amount (2.1 MPa and 1.6 MPa for 70 wt.%).

## CONCLUSION

Based on the results obtained as part of the thesis, which was devoted to the preparation of ER/PDMS and elastomeric (NBR, TPE) composite materials filled with magnetically soft ferrite (MnZn and CI) and the combination of MnZn with carbon fillers with the effects of shielding against electromagnetic radiation, especially of absorption mechanisms, the following conclusions were reached:

- In the case of the ER/PDMS-based composite, the best result was achieved with the ER/PDMS10 matrix. It clearly follows from the calculated  $RL_{\min}$  values that composites with this matrix achieve the best values in terms of  $RL_{\min}$  in the widest frequency range. At the same time, they achieve the best absorption values for MnZn 70 wt.% and CI 70 wt.%. ER/PDMS30 composites also show good values of  $RL_{\min}$  in a wide frequency range, however, these results are no longer significantly different from the values for ER/PDMS10 composites with 70 wt. % filler. From the point of view of optimizing weight and price, their use is not advantageous.
- For composites with elastomeric matrix (TPE), we can observe that the best values of  $RL_{\min}$  in the widest frequency band at the -10 dB level are achieved by the MnZn 70 wt.%. The TPE composites with MnZn 80 wt. % achieves similar  $RL_{\min}$  values leading to higher weights of the final product. We observe a similar result for composites with CI. A composite with a higher filler content (70 wt.%) does not bring any significant improvement of  $RL_{\min}$ . In the case of both types of fillers, it is therefore preferable to use a filler with 70 wt.%.
- Carbon-based fillers have a stiffening effect in rubber compounds, which is reflected in the good strength characteristics of composite materials. The electrical percolation threshold for composites with CB was found at 16 wt. %, which proves that it is a conductive composite. For this reason, it achieves exceedingly low absorption values ( $RL_{\min} \sim -2$  dB).
- The application of CB and CNT in an elastomeric (NBR) composite filled with a combination of these fillers and MnZn ferrite leads to an improvement in the physical-mechanical properties. Composites filled with a combination of MnZn and CB provide absorption shielding efficiency, with a shift of absorption maxima and overall absorption efficiency towards lower frequency regions (1.9 – 0.32 GHz) compared to composites filled only with MnZn ferrite, and at the same time the effective frequency band of absorption shielding narrows. On the other hand, composites filled with a combination of MnZn and CNT are not able to absorb electromagnetic radiation using absorption mechanisms because they do not show absorption maxima below -10 dB, mainly due to their electrical conductivity of CNT and high permittivity.

## REFERENCES

- [1] SEUNG, Han Ryu et al. Absorption-dominant, low reflection EMI shielding materials with integrated metal mesh/TPU/CIP composite. *Chemical Engineering Journal* [online]. 2022, **428**, 131167 [viewed 2022-07-06]. Available from: <https://doi.org/10.1016/j.cej.2021.131167>
- [2] HIRATA, Akimasa. Estimation of Whole-Body Average SAR in Human Models Due to Plane-Wave Exposure at Resonance Frequency. *IEEE transactions on electromagnetic* [online]. 2010, **52**, 41-48 [viewed 2022-07-06]. Available from: <http://dx.doi.org/10.1109/TEM.2009.2035613>
- [3] KRUŽELÁK, Ján et al. Mechanical, Thermal, Electrical Characteristics and EMI Absorption Shielding Effectiveness of Rubber Composites Based on Ferrite and Carbon Fillers. *Polymers-Basel* [online]. 2021, **13**, 2937 [viewed 2022-07-06]. Available from: <https://doi.org/10.3390/polym13172937>
- [4] NASEER, Anam et al. Reinforcement of Electromagnetic Wave Absorption Characteristics in PVDF-PMMA Nanocomposite by intercalation of Carbon Nanofibers. *Electronic Materials Letters* [online]. 2019, **15**, 201-207 [viewed 2022-07-06]. Available from: <https://doi.org/10.1007/s13391-018-00104-9>
- [5] ROZANOV, Konstantin N. Ultimate thickness to bandwidth ratio of radar absorbers. *IEEE Transactions on Antennas and Propagation* [online]. 2000, **48** (8), 1230-1234 [viewed 2022-07-06]. Available from: <http://doi:10.1109/8.884491>
- [6] Microwave absorbing materials. Laird technologies. [online]. [viewed 2022-07-06]. Available from: <http://www.lairdtech.com>
- [7] Ferrite absorbers. TDK RF Solutions Inc. [online]. [viewed 2022-07-06]. Available from: <http://www.tdkrfsolutions.com>
- [8] KAZANTSEVA, Natalia Magnetic Particle-Filled Polymer Microcomposites. In: SABU, Thomas et al. Polymer Composites, Vol. 1: Macro- and Microcomposites. First Edition. *Wiley-VCH Verlag GmbH & Co. KgaA* [online]. 2012, 613-672 [viewed 2022-07-06]. Available from: <ISBN: 978-3-527-32624-2>
- [9] KONG, J. et al. Electromagnetic wave absorption properties of Fe<sub>3</sub>O<sub>4</sub> octahedral nanocrystallines in gigahertz range. *Appl. Phys. A* [online]. 2011, **105**, 351–354 [viewed 2022-07-06]. Available from: <https://doi.org/10.1007/s00339-011-6593-8>
- [10] JURČA, M. et al. Reduced percolation threshold of conductive adhesive through nonuniform filler localization: Monte Carlo simulation and experimental study. *Composites science and technology* [online]. 2021, vol. **214**, 29 108964 [viewed 2022-07-06]. Available from: <https://doi.org/10.1016/j.compscitech.2021.108964>

- [11] QING, Y. et al. Microwave-absorbing and mechanical properties of carbonyl-iron/epoxy- silicone resin coatings. *J. Magn. Magn. Mater.* [online]. 2009, **321**, 25-28 [viewed 2022-07-06]. Available from: <https://doi.org/10.1016/j.jmmm.2008.07.011>
- [12] PINHO, M.S. et al. Performance of radar absorbing materials by waveguide measurements for X- and Ku-band frequencies. *Eur. Polym. J.* [online]. 2002, **38**, 2321e2327 [viewed 2022-07-06]. Available from: [https://doi.org/10.1016/S0014-3057\(02\)00118-0](https://doi.org/10.1016/S0014-3057(02)00118-0)
- [13] FOULGER, Stephen H. Electrical Properties of Composites in the Vicinity of the Percolation Threshold. *Journal of Applied Polymer Science* [online]. 1999, **72**(12), 1573-82 [viewed 2022-07-06]. Available from: [https://doi.org/10.1002/\(SICI\)1097-4628\(19990620\)72:12<1573::AID-APP10>3.0.CO;2-6](https://doi.org/10.1002/(SICI)1097-4628(19990620)72:12<1573::AID-APP10>3.0.CO;2-6)
- [14] FOULGER, Stephen H. Reduced percolation thresholds of immiscible conductive blends. *Journal of Polymer Science Part B: Polymer Physics* [online]. 1999, **37**(15), 1899-1910 [viewed 2022-07-06]. Available from: [https://doi.org/10.1002/\(SICI\)1099-0488\(19990801\)37:15<1899::AID-POLB14>3.0.CO;2-0](https://doi.org/10.1002/(SICI)1099-0488(19990801)37:15<1899::AID-POLB14>3.0.CO;2-0)
- [15] VILČÁKOVÁ, Jarmila et al. Effect of Surfactants and manufacturing methods on the electrical and thermal conductivity of carbon nanotube/silicone composites. *Molecules* [online]. 2012, **17**(11), 13157-74 [viewed 2022-07-06]. Available from: <https://doi.org/10.3390/molecules171113157>
- [16] PARK, Jun Kue et al. Enhanced anomalous magnetization in carbonyl iron by Ni<sup>+</sup> ion beam irradiation. *Scientific Reports* [online]. 2021, **11** [viewed 2022-07-06]. Available from: <https://doi.org/10.1038/s41598-021-99673-3>
- [17] ABSHINOVA, Madina A. et al. Thermomagnetic stability and heat-resistance properties of carbonyl iron filled siloxanes. *Materials Chemistry and Physics* [online]. 2009, **114**, 78-89 [viewed 2022-07-06]. Available from: <https://doi.org/10.1016/j.matchemphys.2008.08.091>
- [18] MIN, Dandan et al. Facile preparation and enhanced microwave absorption properties of flake carbonyl iron/Fe<sub>3</sub>O<sub>4</sub> composite. *Journal of Magnetism and Magnetic Materials* [online]. 2017, **435**, 26-32 [viewed 2022-07-06]. Available from: <https://doi.org/10.1016/j.jmmm.2017.03.065>
- [19] KUMAR, P. et al. 2019. Recent advances in polymer and polymer composites for electromagnetic interference shielding: review and future prospects. *Polym Rev.* [online]. 2019;59(4):687–738 [viewed 2022-07-06]. Available from: <https://doi.org/10.1080/15583724.2019.1625058>
- [20] JIA, L. CH. et al. A Strong and tough polymer–carbon nanotube film for flexible and efficient electromagnetic interference shielding. *J Mater Chem C* [online]. 2017, **5**:8944–8951 [viewed 2022-07-06]. Available from:

<https://doi.org/10.1039/C7TC02259J>

- [21] DAI, K. et al. Electrically conductive carbon black (CB) filled in situ microfibrillar poly(ethylene terephthalate) (PET)/polyethylene (PE) composite with a selective CB distribution. *Polymer* [online]. 2007, **48**(3):849–859 [viewed 2022-07-06]. Available from: <https://doi.org/10.1016/j.polymer.2006.12.026>
- [22] LIM, K. M., et al. Complex Permeability and Electromagnetic Wave Absorption Properties of Amorphous Alloy-epoxy Composites. *Journal of Non-Crystalline Solids* [online]. 2005, **351**, 75–83 [viewed 2022-07-06]. Available from: <https://doi.org/10.1016/j.jnoncrysol.2004.09.025>
- [23] YOSHIDA, T. et al. Evaluation of absorbing characteristics and thermal contact resistance of electromagnetic wave absorbing composite rubber. *IEEJ Transactions on Fundamentals and Materials* [online]. 2012, **132**, 180–186 [viewed 2022-07-06]. Available from: <https://doi.org/10.1541/ieejfms.132.180>
- [24] LOPATIN, A.V. Polymer Magnetic Composites for Microwave Absorbers [online]. 9788073188443. Doctoral Thesis. *Tomas Bata University, Faculty of Technology* [online]. Supervisor Prof. Ing. Petr Sáha, Ph.D. [viewed 2022-07-06]. Available from: <https://vufind.katalog.k.utb.cz/Record/57651>
- [25] BARR, R. et al. ELF and VLF radio waves. *J. Atmospheric Sol.-Terr. Phys.* [online]. 2000, **62**, 1689-1718 [viewed 2022-07-06]. Available from: [https://doi.org/10.1016/S1364-6826\(00\)00121-8](https://doi.org/10.1016/S1364-6826(00)00121-8)
- [26] CHEN, Junfeng et al. High-impedance surface-based broadband absorbers with interference theory. *IEEE Transactions on Antennas and Propagation* [online] 2015, **63**, 4367–4374 [viewed 2022-07-06]. Available from: <https://doi.org/10.1109/TAP.2015.2459138>
- [27] HE, Yun et al Design of an adjustable polarization-independent and wideband electromagnetic absorber. *Journal of Applied Physics* [online]. 2016, **119**, 105103 [viewed 2022-07-06]. Available from: <https://doi.org/10.1063/1.4943593>
- [28] NAITO, Yoshiyuki and SUETAKE, Kunihiro Application of ferrite to electromagnetic wave absorber and its characteristics. *IEEE Transactions on Microwave Theory and Techniques* [online]. 1971, **19**, 65–72 [viewed 2022-07-06]. Available from: <https://doi.org/10.1109/TMTT.1971.1127446>
- [29] HUANG, Xianjun et al. Experimental demonstration of printed graphene nano flakes enabled flexible and conformable wideband radar absorbers. *Scientific Reports* [online]. 2016, **6**, 38197 [viewed 2022-07-06]. Available from: <https://doi.org/10.1038/srep38197>
- [30] AHMADIA, Farzad and IDAB, Nathan A broadband ultrathin metamaterial absorber using tilted parallel strips. *Proceedings SPIE*



- [online]. 2017, **10103**, 101031V–1 [viewed 2022-07-06]. Available from: <https://doi.org/10.1117/12.2254479>
- [31] MUNAGA, Praneeth et al. A fractal-based compact broadband polarization insensitive metamaterial absorber using lumped resistors. *Microwave and Optical Technology Letters* [online]. 2016, **58**, 343–347 [viewed 2022-07-06]. Available from: <https://doi.org/10.1002/mop.29571>
- [32] WANG, Han et al. Broadband tunability of polarization-insensitive absorber based on frequency selective surface. *Scientific Reports* [online]. 2016, **6**, 23081 [viewed 2022-07-06]. Available from: <https://doi.org/10.1038/srep23081>
- [33] LI, Z. et al. Theoretical Study of Electromagnetic Interference Shielding of 2D MXenes Films. *Metals* [online]. 2018, **8**, 652 [viewed 2022-07-06]. Available from: <https://doi.org/10.3390/met8080652>
- [34] LOPATIN, A.V. et al. The efficiency of application of magnetic polymer composites as radio-absorbing materials. *Journal of Communications Technology and Electronics* [online]. 2008, **53**, 487–496 [viewed 2022-07-06]. Available from: <https://doi.org/10.1134/S106422690805001X>
- [35] GE, Y. et al. ZnFe<sub>2</sub>O<sub>4</sub>@PDA@Polypyrrole composites with efficient electromagnetic wave absorption properties in the 18–40 GHz region. *Journal of Materials Science* [online]. 2021, **56**, 10876–10891 [viewed 2022-07-06]. Available from: <https://doi.org/10.1007/s10853-021-05968-1>
- [36] SANKARAN, S. et al. Recent advances in electromagnetic interference shielding properties of metal and carbon filler reinforced flexible polymer composites: A review. *Composites Part A: Applied Science and Manufacturing* [online]. 2018, **S. 114**, 49–71 [viewed 2022-07-06]. Available from: <https://doi.org/10.1016/j.compositesa.2018.08.006>
- [37] JAROSZEWSKI, M. et al. Advanced Materials for Electromagnetic Shielding. Fundamentals, Properties and Applications. *John Wiley & Sons, Inc. 1st Ed.* [online]. 2019 [viewed 2022-07-06]. Available from: <https://doi.org/10.1002/9781119128625>
- [38] FISKE, T. J. et al. Percolation in magnetic composites. *Journal of Materials Science* [online]. 1997, **32**(20), 5551–60 [viewed 2022-07-06]. Available from: <https://doi.org/10.1023/A:1018620407013>
- [39] YADAV, Raghvendra Singh et al. Advanced Spinel Ferrite Nanocomposites for Electromagnetic Interference Shielding Applications. 2020, *Elsevier Inc. Netherlands* [online]. [viewed 2022-07-06]. Available from: <https://www.elsevier.com/books-and-journals>
- [40] MOUČKA, Robert et al. Enhancement of magnetic losses in hybrid polymer composites with MnZn-ferrite and conducting fillers. *Journal of Material Science* [online]. 2007, **42**, 9480–90 [viewed 2022-07-06]. Available from: <https://doi.org/10.1007/s10853-007-2081-0>

- [41] LAGARKOV, Andrey N. et al. High-frequency behavior of magnetic composites. *Journal of Magnetism and Magnetic Materials* [online] 2009, **321**(14), 2082-92 [viewed 2022-07-06]. Available from: <https://doi.org/10.1016/j.jmmm.2008.08.099>
- [42] SISTA, Kameswara Srikar et al. Carbonyl iron powders as absorption material for microwave interference shielding: A review. *Journal of Alloys and Compounds* [online]. 2021, **853** [viewed 2022-07-06]. Available from: <https://doi.org/10.1016/j.jallcom.2020.157251>
- [43] BATEL, Lotfi et al. Tunable Magneto-Dielectric Material for Electrically Small and Reconfigurable Antenna Systems at Vhf Band. *Ceramics* [online]. 2020, **3** (3), 276-286 [viewed 2022-07-06]. Available from: <https://doi.org/10.3390/ceramics3030025>
- [44] KRUŽELÁK, J. et al. Electromagnetic Interference Shielding and Physical-Mechanical Characteristics of Rubber Composites Filled with Manganese-Zinc Ferrite and Carbon Black. *Polymers* [online]. 2021, **13** (4), 616 [viewed 2022-07-06]. Available from: <https://doi.org/10.3390/polym13040616>
- [45] [www.jvmicronics.co](http://www.jvmicronics.co) [online]. [viewed 2022-07-06]. Available from: <https://www.jvmicronics.co.in/rf-absorber.html>
- [46] KRUŽELÁK, J. et al. 2021. Progress in polymers and polymer composites used as efficient materials for EMI shielding. *In Nanoscale Adv.* [online]. 2021, vol. 3, p. 123–172 [viewed 2022-07-06]. Available from: <https://doi.org/10.1039/D0NA00760A>
- [47] AL-SALEH, M.H. et al. EMI shielding effectiveness of carbon based nanostructured polymeric materials: A comparative study. *Carbon* [online]. 2013, **60**, 146–156 [viewed 2022-07-06]. Available from: <https://doi.org/10.1016/j.carbon.2013.04.008>
- [48] ZHU, J. et al. Carbon nanostructure-derived polyaniline metacomposites: Electrical, dielectric, and giant magnetoresistive properties. *Langmuir* [online] 2012, **28**, 10246–10255 [viewed 2022-07-06]. Available from: <https://doi.org/10.1021/la302031f>
- [49] GOŘALÍK, M. et al. Engineering Magnetic Type Radio-Absorbers Based on Composites with a Dual-Phase Polymer Matrix. *Electronic Materials Letters* [online]. 2022 [viewed 2022-07-06]. Available from: <https://doi.org/10.1007/s13391-022-00351-x>
- [50] JANI, R. K. et al. Tuning of microwave absorption properties and electromagnetic interference (EMI) shielding effectiveness of nanosize conducting black-silicone rubber composites over 8–18 GHz. *Prog Electromang Res* [online]. 2017, **58**:193–204 [viewed 2022-07-06]. Available from: <https://doi.org/10.2528/PIERM17022704>

- [51] KRUŽELÁK, J. et al. Cross-linking, mechanical, dynamical, and EMI absorption shielding effectiveness of NBR based composites filled with combination on ferrite and carbon based fillers. *Polymers Advanced Technologies* [online]. 2021, 1-11 [viewed 2022-07-06]. Available from: <https://doi.org/10.1002/pat.5305>
- [52] <https://hollandshielding.com> [online] [viewed 2022-07-06]. Available from: <https://hollandshielding.com/Nonflammable-high-power-handling-absorbers>
- [53] [www.jvmicronics.co](http://www.jvmicronics.co) [online]. [viewed 2022-07-06]. Available from: <https://www.jvmicronics.co.in/rf-absorber.html>
- [54] [wikimedia.org](https://commons.wikimedia.org) [online] [viewed 2022-07-06]. Available from: [https://commons.wikimedia.org/wiki/File:Electromagnetic\\_spectrum\\_with\\_sources.svg](https://commons.wikimedia.org/wiki/File:Electromagnetic_spectrum_with_sources.svg)

## LIST OF FIGURES

Figure 1: Dependence of Young's modulus on density

Figure 2: Dependence of tensile strength on price (CZK/kg)

Figure 3: EWAs: a) pyramidal type, b) plane type, c) honeycomb type.

Figure 4: EM band applications in the (RF) and (MW) range.

Figure 5: The interaction of electromagnetic waves with the material.

Figure 6: Free-space measurement method a) A two-port (A) PNA-L network analyser (N5230A) b) antennas c) calibration plates.

Figure 7: The SEM micrographs of the magnetic filler: a) MnZn ferrite b) CI.

Figure 8: The SEM micrographs of the composites: a) ER/MnZn50 b) ER/CI50 c) ER/PDMS10/CI70 d) ER/PDMS10/CI80.

Figure 9: SEM images of NBR composite a) filled with 500 phr of MnZn, b) NBR composites based on 20 phr CB and 300 phr MnZn, c) NBR composites based on 20 phr CB.

Figure 11: The frequency dependences of the complex permittivity of the polymer composites filled with a) MnZn and b) CI (wt. %).

Figure 12: Frequency dependences of real  $\epsilon'$  and imaginary  $\epsilon''$  parts of complex permittivity for a) NBR composites filled with ferrite MnZn, b) hybrid NBR/CB/MnZn composites.

Figure 13: The frequency dependence of the complex magnetic permeability of the polymer composites filled with a) MnZn and b) CI (wt. %).

Figure 14: The effect of the filler concentration on the field internal demagnetizing in the magnetic composites: a) 50 wt. % magnetic filler b) 70 wt. % magnetic filler.

Figure 15: Frequency dependences of real  $\mu'$  and imaginary  $\mu''$  parts of complex permeability for a) MnZn filled NBR composites, b) CB20/MnZn filled NBR composites.

Figure 16: The frequency dependence of the reflection loss of the composites filled with 50 wt. % MnZn based on: a) ER b) ER/PDMS10 and c) ER/PDMS30.

Figure 17: The frequency dependences of the reflection loss of the composites filled with MnZn (36 vol. % = 70 wt. %) and CI (36 vol. % = 80 wt. %) based on: a) ER b) ER/PDMS10 and c) ER/PDMS30.

Figure 18: Frequency dependences of RL for a) NBR composites filled with MnZn, b) hybrid CB/MnZn NBR composites.

Figure 19: The frequency dependence of the reflection loss of the TPE

composites filled with a) MnZn, b) CI.

Figure 20: The temperature dependences of a) the storage modulus  $E'$  b)  $\tan \delta$  of the composite filled by CI and c) XPS of the ER/PDMS10/CI80.

Figure 21: Temperature dependences of  $\tan \delta$  for CB/MnZn NBR composites.

Figure 22: Tensile strength of a) hybrid NCB20/MnZn and CNT/MnZn NBR composites, b) TPE/MnZn and TPE/CI composites.

Figure 23: The concentration dependence of DC electrical conductivity on a) ER/MnZn and ER/PDMS/MnZn composites, b) TPE/MnZn and TPE/CI composites

Figure 24: The concentration dependence of DC electrical conductivity on NBR/MnZn and hybrid NBR/CB20/MnZn, NBR/CNT5/MnZn composites.

## **LIST OF TABLES**

Table 1: Physical-mechanical properties of selected matrix

Table 2: Basic properties of fillers

## LIST OF SYMBOLS AND ABBREVIATIONS

DGEBA	diglycidyl ether bisphenol A
PDMS	polydimethylsiloxane
DETA	diethylenetriamine
DCP	dicumyl peroxide
MPS	multiphase polymer systems
DMA	dynamical mechanical analysis
RF	radio frequency
$\sigma$	electrical conductivity
$\epsilon^*$	complex permittivity
$\epsilon'$	real part of complex permittivity
$\epsilon''$	imaginary part of complex permittivity
$\mu^*$	complex permeability
$\mu'$	real part of complex permeability
$\mu''$	imaginary part of complex permeability
$\delta$	skin depth
ER	epoxy resin
NBR	acrylonitrile-butadiene rubber
TPE	thermoplastic elastomer
iPP	isostatic propylene
CPC	conductive polymer composite
CB	carbon black
CNT	carbon nanotubes
SWNT	single-wall nanotubes
MWNT	multi-wall nanotubes
T <sub>g</sub>	glass transition temperature
E'	dynamic storage modulus
RL	reflection loss

SE	shielding effectiveness
SE <sub>R</sub>	shielding effectiveness reflection
SE <sub>A</sub>	shielding effectiveness absorptin
$\lambda$	wave length
MnZn	manganese-zinc
CI	carbonyl iron
PC	percolation threshold
wt. %	weight concentration
vol. %	volume concentration
SEM	scanning electron microscopy
EMI	electromagnetic interference
EWA	electromagnetic wave absorbers
EPC	electromagnetic polymer composites
RA	radio absorber
RAM	radio absorbing material
SAR	specific absorption rate

# CURRICULUM VITAE

## Personal information

Name	Marek Gořalík
Address	Martinice 170, 769 01, Czech Republic
Telephone	+420 732 450 785
E-mail	<a href="mailto:goralik@ft.utb.cz">goralik@ft.utb.cz</a> , mgoralik@gmail.com
Nationality	Czech
Date of birth	12. 03. 1979

## Education and training

Dates	2014 – present
Title of qualification awarded	Doctoral study – expected defence 2022
Principal branch	Technology of Macromolecular Substances
Organisation providing education	Centre of Polymer Systems – Tomas Bata University in Zlín

Dates	2001–2004
Title of qualification awarded	Ing.
Principal branch	Chemistry and Materials Technology
Organisation providing education	Faculty of Technology – Tomas Bata University in Zlín

Dates	1998-2001
Title of qualification awarded	Bc.
Principal branch	Chemistry and Materials Technology
Organisation providing education	Faculty of Technology – Tomas Bata University in Zlín



## LIST OF PUBLICATIONS

1. **GOŘALÍK, M.**, JURČA, M., BUBULINCA, C., BABAYAN, V.A., VILČÁKOVÁ, J., KAZANTSEVA, N.E., SÁHA, P. Engineering Magnetic Type Radio-Absorbers Based on Composites with a Dual-Phase Polymer Matrix. *Electronic Materials Letters*. 2022, **18**, p. 345-360. <https://doi.org/10.1007/s13391-022-00351-x>
2. YADAV, R.S., KUŘITKA I., VILČÁKOVÁ, J., MACHOVSKÝ, M., ŠKODA, D., URBÁNEK, P., MASAŘ, M., **GOŘALÍK, M.**, URBÁNEK M., KALINA L., and HAVLICA J. Polypropylene Nanocomposite Filled with Spinel Ferrite NiFe<sub>2</sub>O<sub>4</sub> Nanoparticles and In-Situ Thermally-Reduced Graphene Oxide for Electromagnetic Interference Shielding Application. *Nanomaterials*. 2019, **9**(4), p. 621 - 674. <https://doi.org/10.3390/nano9040621>
3. STEJSKAL, J., SAPURINA, I., VILČÁKOVÁ, J., PLACHÝ, T., SEDLAČÍK, M., BUBULINCA, C., **GOŘALÍK, M.**, TRCHOVÁ, M., KOLSKÁ, Z., and PROKEŠ, J. Conducting and Magnetic Composites Polypyrrole Nanotubes/Magnetite Nanoparticles: Application in Magnetorheology. *Applied Nano Materials*. 2021, **4**, 2247-2256. <https://dx.doi.org/10.1021/acsanm.1c00063>
4. KRUŽELÁK, J., MEDLENOVÁ, E., KVASNIČÁKOVÁ, A., DOSOUDIL R. HUDEC, I., and **GOŘALÍK, M.** Rubber Magnetic Composites Cross-Linked with Peroxide Curing Systems. *Polymer Science Series B*. 2019, **61**(6), 865-873. <https://doi.org/10.1134/S1560090419060071>
5. KVASNIČÁKOVÁ, A., KRUŽELÁK, J., MEDLENOVÁ, E., DOSOUDIL, R., HUDEC, I., and **GOŘALÍK, M.** Rubber magnets cured with peroxide and coagents. *Journal of Elastomers And Plastics*. 2020, **52**(3), 253-270. <https://doi.org/10.1177/0095244319846176>
6. JURČA, M., VILČÁKOVÁ, J., **GOŘALÍK, M.**, MASAŘ, M., PONÍŽIL, P., KAZANTSEVA, N., FOULGER, S. H. and SÁHA, P. Reduced percolation threshold of conductive adhesive through nonuniform filler localization: Monte Carlo simulation and experimental study. *Composites Science and Technology*. 2021, **214**. doi: <https://doi.org/10.1016/j.compscitech.2021.108964>.
7. KRUŽELÁK, J., KVASNIČÁKOVÁ, A., HLOŽEKOVÁ, K., DOSOUDIL, R., **GOŘALÍK, M.**, and HUDEC, I. Electromagnetic

Interference Shielding and Physical-Mechanical Characteristics of Rubber Composites Filled with Manganese-Zinc Ferrite and Carbon Black. *Polymers*. 2021, **13** (4), 616. <https://doi.org/10.3390/polym13040616>

8. KRUŽELÁK, J., KVASNIČÁKOVÁ, A., BOCHKAREV, E. S., TUZHIKOV, O.O., **GOŘALÍK, M.**, VILČÁKOVÁ, J., and HUDEC, I. Cross-linking, mechanical, dynamical, and EMI absorption shielding effectiveness of NBR based composites filled with combination on ferrite and carbon based fillers. *Polymers Advanced Technologies*. 2021, 1-11. <https://doi.org/10.1002/pat.5305>
9. KRUŽELÁK, J., KVASNIČÁKOVÁ, A, HLOŽEKOVÁ, K., PLAVES, R., DOSOUDIL, R., **GOŘALÍK, M.**, VILČÁKOVÁ, J., and HUDEC, I. Mechanical, Thermal, Electrical Characteristics and EMI Absorption Shielding Effectiveness of Rubber Composites Based on Ferrite and Carbon Fillers. *Polymers*. 2021, **13** (17), 2937. <https://doi.org/10.3390/polym13172937>

## OVERVIEW OF OTHER ACTIVITIES

### *Conference:*

JURČA M., **GOŘALÍK M.**, VILČÁKOVÁ J., FOULGER S.H., MASAŘ M. and KAZANTSEVA N. (2019), Enhanced electrical conductivity of immiscible blends filled with nickel particles. *ACS National Meeting Orlando*.

### *Studies abroad:*

Doctoral study stays at the Institute of Natural and Synthetic Polymers at the Slovak University of Technology in Bratislava (Slovak Republic) 08/2021 - 09/2021

# **Vlastnosti polymerních kompozitů pohlcujících elektromagnetické vlny**

Electromagnetic wave absorbing properties of polymer composites

Doctoral Thesis Summary

Published by: Tomas Bata University in Zlín  
nám. T. G. Masaryka 5555, 760 01 Zlín.

Edition: published electronically

Typesetting by: Ing. Marek Gořalík, Ph.D.

This publication has not undergone any proofreading or editorial review.

Publication year: 2022

ISBN 978-80-7678-116-0

